DESY 01–021
February 2001

ISSN 0418–9833

Searches at HERA for Squarks in R-Parity Violating Supersymmetry

H1 Collaboration

Abstract

A search for squarks in R-parity violating supersymmetry is performed in e^+p collisions at HERA at a centre of mass energy of 300 GeV, using H1 data corresponding to an integrated luminosity of 37 pb^{-1}. The direct production of single squarks of any generation in positron-quark fusion via a Yukawa coupling λ' is considered, taking into account R-parity violating and conserving decays of the squarks. No significant deviation from the Standard Model expectation is found. The results are interpreted in terms of constraints within the Minimal Supersymmetric Standard Model (MSSM), the constrained MSSM and the minimal Supergravity model, and their sensitivity to the model parameters is studied in detail. For a Yukawa coupling of electromagnetic strength, squark masses below 260 GeV are excluded at 95% confidence level in a large part of the parameter space. For a 100 times smaller coupling strength masses up to 182 GeV are excluded.

To be submitted to *Eur. Phys. J. C*

C. Adloff[33], V. Andreev[24], B. Andrieu[27], T. Anthonis[4], V. Arkadov[35], A. Astvatsatourov[35], I. Ayyaz[28], A. Babaev[23], J. Bähr[35], P. Baranov[24], E. Barrelet[28], W. Bartel[10], U. Bassler[28], P. Bate[21], A. Beglarian[34], O. Behnke[13], C. Beier[14], A. Belousov[24], T. Benisch[10], Ch. Berger[1], G. Bernardi[28], T. Berndt[14], J.C. Bizot[26], V. Boudry[27], W. Braunschweig[1], V. Brisson[26], H.-B. Bröker[2], D.P. Brown[11], W. Brückner[12], P. Bruel[27], D. Bruncko[16], J. Bürger[10], F.W. Büsser[11], A. Bunyatyan[12,34], H. Burkhardt[14], A. Burrage[18], G. Buschhorn[25], A.J. Campbell[10], J. Cao[26], T. Carli[25], S. Caron[1], D. Clarke[5], B. Clerbaux[4], C. Collard[4], J.G. Contreras[7,41], Y.R. Coppens[3], J.A. Coughlan[5], M.-C. Cousinou[22], B.E. Cox[21], G. Cozzika[9], J. Cvach[29], J.B. Dainton[18], W.D. Dau[15], K. Daum[33,39], M. Davidsson[20], B. Delcourt[26], N. Delerue[22], R. Demirchyan[34], A. De Roeck[10,43], E.A. De Wolf[4], C. Diaconu[22], J. Dingfelder[13], P. Dixon[19], V. Dodonov[12], J.D. Dowell[3], A. Droutskoi[23], A. Dubak[25], C. Duprel[2], G. Eckerlin[10], D. Eckstein[35], V. Efremenko[23], S. Egli[32], R. Eichler[36], F. Eisele[13], E. Eisenhandler[19], M. Ellerbrock[13], E. Elsen[10], M. Erdmann[10,40,e], W. Erdmann[36], P.J.W. Faulkner[3], L. Favart[4], A. Fedotov[23], R. Felst[10], J. Ferencei[10], S. Ferron[27], M. Fleischer[10], Y.H. Fleming[3], G. Flügge[2], A. Fomenko[24], I. Foresti[37], J. Formánek[30], J.M. Foster[21], G. Franke[10], E. Gabathuler[18], K. Gabathuler[32], J. Garvey[3], J. Gassner[32], J. Gayler[10], R. Gerhards[10], C. Gerlich[13], S. Ghazaryan[34], L. Goerlich[6], N. Gogitidze[24], M. Goldberg[28], C. Goodwin[3], C. Grab[36], H. Grässler[2], T. Greenshaw[18], G. Grindhammer[25], T. Hadig[13], D. Haidt[10], L. Hajduk[6], W.J. Haynes[5], B. Heinemann[18], G. Heinzelmann[11], R.C.W. Henderson[17], S. Hengstmann[37], H. Henschel[35], R. Heremans[4], G. Herrera[7,41], I. Herynek[29], M. Hildebrandt[37], M. Hilgers[36], K.H. Hiller[35], J. Hladký[29], P. Höting[2], D. Hoffmann[22], R. Horisberger[32], S. Hurling[10], M. Ibbotson[21], Ç. İşsever[7], M. Jacquet[26], M. Jaffre[26], L. Janauschek[25], D.M. Jansen[12], X. Janssen[4], V. Jemanov[11], L. Jönsson[20], D.P. Johnson[4], M.A.S. Jones[18], H. Jung[20,10], H.K. Kästli[36], D. Kant[19], M. Kapichine[8], M. Karlsson[20], O. Karschnick[11], F. Keil[14], N. Keller[37], J. Kennedy[18], I.R. Kenyon[3], S. Kermiche[22], C. Kiesling[25], P. Kjellberg[20], M. Klein[35], C. Kleinwort[10], G. Knies[10], B. Koblitz[25], S.D. Kolya[21], V. Korbel[10], P. Kostka[35], S.K. Kotelnikov[24], R. Koutouev[12], A. Koutov[8], H. Krehbiel[10], J. Kroseberg[37], K. Krüger[10], A. Küpper[33], T. Kuhr[11], T. Kurča[25,16], R. Lahmann[10], D. Lamb[3], M.P.J. Landon[19], W. Lange[35], T. Laštovička[35], P. Laycock[18], E. Lebailly[26], A. Lebedev[24], B. Leißner[1], R. Lemrani[10], V. Lendermann[7], S. Levonian[10], M. Lindstroem[20], B. List[36], E. Lobodzinska[10,6], B. Lobodzinski[6,10], A. Loginov[23], N. Loktionova[24], V. Lubimov[23], S. Lüders[36], D. Lüke[7,10], L. Lytkin[12], N. Magnussen[33], H. Mahlke-Krüger[10], N. Malden[21], E. Malinovski[24], I. Malinovski[24], R. Maraček[25], P. Marage[4], J. Marks[13], R. Marshall[21], H.-U. Martyn[1], J. Martyniak[6], S.J. Maxfield[18], D. Meer[36], A. Mehta[18], K. Meier[14], P. Merkel[10], A.B. Meyer[11], H. Meyer[33], J. Meyer[10], P.-O. Meyer[2], S. Mikocki[6], D. Milstead[18], T. Mkrtchyan[34], R. Mohr[25], S. Mohrdieck[11], M.N. Mondragon[7], F. Moreau[27], A. Morozov[8], J.V. Morris[5], K. Müller[37], P. Murín[16,42], V. Nagovizin[23], B. Naroska[11], J. Naumann[7], Th. Naumann[35], G. Nellen[25], P.R. Newman[3], T.C. Nicholls[5], F. Niebergall[11], C. Niebuhr[10], O. Nix[14], G. Nowak[6], T. Nunnemann[12], J.E. Olsson[10], D. Ozerov[23], V. Panassik[8], C. Pascaud[26], G.D. Patel[18], M. Peez[22], E. Perez[9], J.P. Phillips[18], D. Pitzl[10], R. Pöschl[7], I. Potachnikova[12], B. Povh[12], K. Rabbertz[1], G. Rädel[1], J. Rauschenberger[11], P. Reimer[29], B. Reisert[25], D. Reyna[10], S. Riess[11], C. Risler[25], E. Rizvi[3], P. Robmann[37], R. Roosen[4], A. Rostovtsev[23], C. Royon[9], S. Rusakov[24], K. Rybicki[6], D.P.C. Sankey[5], J. Scheins[1], F.-P. Schilling[13], P. Schleper[10], D. Schmidt[33], D. Schmidt[10], S. Schmitt[10], M. Schneider[22], L. Schoeffel[9], A. Schöning[36], T. Schörner[25], V. Schröder[10], H.-C. Schultz-Coulon[7], C. Schwanenberger[10], K. Sedlák[29], F. Sefkow[37], V. Shekelyan[25], I. Sheviakov[24], L.N. Shtarkov[24], Y. Sirois[27], T. Sloan[17], P. Smirnov[24], V. Solochenko[23,†], Y. Soloviev[24], V. Spaskov[8], A. Specka[27], H. Spitzer[11], R. Stamen[7], J. Steinhart[10], B. Stella[31], A. Stellberger[14], J. Stiewe[14], U. Straumann[37], W. Struczinski[2], M. Swart[14], M. Taševský[29], V. Tchernyshov[23], S. Tchetchelnitski[23], G. Thompson[19], P.D. Thompson[3], N. Tobien[10], D. Traynor[19], P. Truöl[37], G. Tsipolitis[10,38], I. Tsurin[35], J. Turnau[6], J.E. Turney[19], E. Tzamariudaki[25], S. Udluft[25], A. Usik[24], S. Valkár[30], A. Valkárová[30], C. Vallée[22], P. Van Mechelen[4], S. Vassiliev[8], Y. Vazdik[24], A. Vichnevski[8], K. Wacker[7], R. Wallny[37], T. Walter[37], B. Waugh[21], G. Weber[11], M. Weber[14], D. Wegener[7], M. Werner[13], N. Werner[37], G. White[17], S. Wiesand[33], T. Wilksen[10], M. Winde[35], G.-G. Winter[10], Ch. Wissing[7], M. Wobisch[2], H. Wollatz[10], E. Wünsch[10], A.C. Wyatt[21], J. Žáček[30], J. Zálešák[30], Z. Zhang[26], A. Zhokin[23], F. Zomer[26], J. Zsembery[9], and M. zur Nedden[10]

[1] *I. Physikalisches Institut der RWTH, Aachen, Germany*[a]
[2] *III. Physikalisches Institut der RWTH, Aachen, Germany*[a]
[3] *School of Physics and Space Research, University of Birmingham, Birmingham, UK*[b]
[4] *Inter-University Institute for High Energies ULB-VUB, Brussels; Universitaire Instelling Antwerpen, Wilrijk; Belgium*[c]
[5] *Rutherford Appleton Laboratory, Chilton, Didcot, UK*[b]
[6] *Institute for Nuclear Physics, Cracow, Poland*[d]
[7] *Institut für Physik, Universität Dortmund, Dortmund, Germany*[a]
[8] *Joint Institute for Nuclear Research, Dubna, Russia*
[9] *CEA, DSM/DAPNIA, CE-Saclay, Gif-sur-Yvette, France*
[10] *DESY, Hamburg, Germany*[a]
[11] *II. Institut für Experimentalphysik, Universität Hamburg, Hamburg, Germany*[a]
[12] *Max-Planck-Institut für Kernphysik, Heidelberg, Germany*[a]
[13] *Physikalisches Institut, Universität Heidelberg, Heidelberg, Germany*[a]
[14] *Kirchhoff-Institut für Physik, Universität Heidelberg, Heidelberg, Germany*[a]
[15] *Institut für experimentelle und Angewandte Physik, Universität Kiel, Kiel, Germany*[a]
[16] *Institute of Experimental Physics, Slovak Academy of Sciences, Košice, Slovak Republic*[e,f]
[17] *School of Physics and Chemistry, University of Lancaster, Lancaster, UK*[b]
[18] *Department of Physics, University of Liverpool, Liverpool, UK*[b]
[19] *Queen Mary and Westfield College, London, UK*[b]
[20] *Physics Department, University of Lund, Lund, Sweden*[g]
[21] *Physics Department, University of Manchester, Manchester, UK*[b]
[22] *CPPM, CNRS/IN2P3 - Univ Mediterranee, Marseille - France*
[23] *Institute for Theoretical and Experimental Physics, Moscow, Russia*
[24] *Lebedev Physical Institute, Moscow, Russia*[e,h]
[25] *Max-Planck-Institut für Physik, München, Germany*[a]
[26] *LAL, Université de Paris-Sud, IN2P3-CNRS, Orsay, France*
[27] *LPNHE, Ecole Polytechnique, IN2P3-CNRS, Palaiseau, France*
[28] *LPNHE, Universités Paris VI and VII, IN2P3-CNRS, Paris, France*
[29] *Institute of Physics, Czech Academy of Sciences, Praha, Czech Republic*[e,i]
[30] *Faculty of Mathematics and Physics, Charles University, Praha, Czech Republic*[e,i]
[31] *Dipartimento di Fisica Università di Roma Tre and INFN Roma 3, Roma, Italy*
[32] *Paul Scherrer Institut, Villigen, Switzerland*
[33] *Fachbereich Physik, Bergische Universität Gesamthochschule Wuppertal, Wuppertal, Germany*[a]
[34] *Yerevan Physics Institute, Yerevan, Armenia*
[35] *DESY, Zeuthen, Germany*[a]
[36] *Institut für Teilchenphysik, ETH, Zürich, Switzerland*[j]
[37] *Physik-Institut der Universität Zürich, Zürich, Switzerland*[j]
[38] *Also at Physics Department, National Technical University, Zografou Campus, GR-15773 Athens, Greece*
[39] *Also at Rechenzentrum, Bergische Universität Gesamthochschule Wuppertal, Germany*
[40] *Also at Institut für Experimentelle Kernphysik, Universität Karlsruhe, Karlsruhe, Germany*
[41] *Also at Dept. Fis. Ap. CINVESTAV, Mérida, Yucatán, México*[k]
[42] *Also at University of P.J. Šafárik, Košice, Slovak Republic*
[43] *Also at CERN, Geneva, Switzerland*

† *Deceased*

[a] *Supported by the Bundesministerium für Bildung, Wissenschaft, Forschung und Technologie, FRG, under contract numbers 7AC17P, 7AC47P, 7DO55P, 7HH17I, 7HH27P, 7HD17P, 7HD27P, 7KI17I, 6MP17I and 7WT87P*
[b] *Supported by the UK Particle Physics and Astronomy Research Council, and formerly by the UK Science and Engineering Research Council*
[c] *Supported by FNRS-NFWO, IISN-IIKW*
[d] *Partially Supported by the Polish State Committee for Scientific Research, grant no. 2P0310318 and SPUB/DESY/P03/DZ-1/99, and by the German Federal Ministry of Education and Science, Research and Technology (BMBF)*
[e] *Supported by the Deutsche Forschungsgemeinschaft*
[f] *Supported by VEGA SR grant no. 2/5167/98*
[g] *Supported by the Swedish Natural Science Research Council*
[h] *Supported by Russian Foundation for Basic Researc grant no. 96-02-00019*
[i] *Supported by GA AV ČR grant no. A1010821*
[j] *Supported by the Swiss National Science Foundation*
[k] *Supported by CONACyT*

1 Introduction

Supersymmetry (SUSY) relates elementary fermions and bosons and protects the mass of the Higgs boson from acquiring unnaturally large radiative corrections. SUSY is often considered an ingredient of a fundamental theory beyond the Standard Model (SM). It is thus actively searched for in current experiments.

The ep collider HERA which provides both baryonic and leptonic quantum numbers in the initial state is ideally suited to search for new particles possessing couplings to an electron-quark pair. Such particles could be squarks, the scalar SUSY partners of quarks, in models where R-parity, a discrete symmetry related to lepton and baryon number conservation, is violated ($\not R_p$). These squarks could thus be resonantly produced at HERA via the fusion of the initial state positron of energy 27.5 GeV with a quark coming from the incident proton of energy 820 GeV, up to the centre of mass energy $\sqrt{s} \simeq 300$ GeV.

In this paper, a search is performed for squarks that are singly produced via an $\not R_p$ coupling, considering both $\not R_p$ decays and decays via gauge couplings involving neutralinos, charginos or gluinos. The data were taken from 1994 to 1997 and correspond to an integrated luminosity of 37 pb^{-1}. This analysis extends the searches for eq resonances previously performed by H1 [1] using the same data sample by considering specific squark decay modes, and supersedes earlier published dedicated squark searches [2, 3] which were based on $\sim$ 13 times less data.

2 Phenomenology

The most general SUSY theory which preserves the gauge invariance of the Standard Model allows for Yukawa couplings between two known SM fermions and the scalar SUSY partner of a quark (a squark $\tilde{q}$) or of a lepton (a slepton $\tilde{l}$). Such couplings induce violation of the R-parity defined as $R_p = (-1)^{3B+L+2S}$, where S denotes the spin, B the baryon number and L the lepton number of the particles. Hence R_p is equal to 1 for particles and equal to -1 for sparticles. We consider here the SUSY phenomenology at HERA in the presence of $\not R_p$ Yukawa couplings but maintain otherwise the minimal field content of the Minimal Supersymmetric Standard Model (MSSM) [4]. Of special interest for HERA are the Yukawa couplings between a squark and a lepton-quark pair [5]. These are described in the superpotential by the terms $\lambda'_{ijk} L_i Q_j \bar{D}_k$, with i, j, k being generation indices[1]. The corresponding part of the Lagrangian, expanded in fields, reads as:

$$\begin{aligned}\mathcal{L}_{L_i Q_j \bar{D}_k} &= \lambda'_{ijk}\left[-\tilde{e}^i_L u^j_L \bar{d}^k_R - e^i_L \tilde{u}^j_L \bar{d}^k_R - (\bar{e}^i_L)^c u^j_L \tilde{d}^{k*}_R \right.\\ &\quad \left. +\tilde{\nu}^i_L d^j_L \bar{d}^k_R + \nu_L \tilde{d}^j_L \bar{d}^k_R + (\bar{\nu}^i_L)^c d^j_L \tilde{d}^{k*}_R\right] + \text{c.c.} \qquad (1)\end{aligned}$$

where the superscripts c denote the charge conjugate spinors and the $*$ the complex conjugate of scalar fields. Hence the couplings λ'_{1jk} allow for resonant production of squarks at HERA through eq fusion. For the nine possible λ'_{1jk} couplings, the corresponding single production processes are given in table 1. With an e^+ beam, HERA is most sensitive to couplings λ'_{1j1}, where mainly $\tilde{u}^j_L$ squarks are being produced with a cross-section approximately scaling as

[1] In the usual superfield notation, L_i, Q_j and D_k contain respectively the left-handed leptons, the left-handed quarks and the right-handed down quark, together with their SUSY partners $\tilde{l}^i_L$, $\tilde{q}^j_L$ and $\tilde{d}^k_R$.

Table 1: The two resonant squark production processes at HERA (e^+ beam) allowed by each R-parity violating coupling λ'_{1jk}.

λ'_{1jk}	production process	
111	$e^+ + \bar{u} \to \overline{\tilde{d}_R}$	$e^+ + d \to \tilde{u}_L$
112	$e^+ + \bar{u} \to \overline{\tilde{s}_R}$	$e^+ + s \to \tilde{u}_L$
113	$e^+ + \bar{u} \to \overline{\tilde{b}_R}$	$e^+ + b \to \tilde{u}_L$
121	$e^+ + \bar{c} \to \overline{\tilde{d}_R}$	$e^+ + d \to \tilde{c}_L$
122	$e^+ + \bar{c} \to \overline{\tilde{s}_R}$	$e^+ + s \to \tilde{c}_L$
123	$e^+ + \bar{c} \to \overline{\tilde{b}_R}$	$e^+ + b \to \tilde{c}_L$
131	$e^+ + \bar{t} \to \overline{\tilde{d}_R}$	$e^+ + d \to \tilde{t}_L$
132	$e^+ + \bar{t} \to \overline{\tilde{s}_R}$	$e^+ + s \to \tilde{t}_L$
133	$e^+ + \bar{t} \to \overline{\tilde{b}_R}$	$e^+ + b \to \tilde{t}_L$

$\lambda'^2_{1j1} \cdot d(x)$ where $d(x)$ is the probability to find a d quark in the proton with a momentum fraction $x = M^2_{\tilde{q}}/s$ and $M_{\tilde{q}}$ denotes the squark mass. The production of the antisquark $\overline{\tilde{d}^k_R}$ is also possible albeit with a much lower cross-section since a $\bar{u}^j$ antiquark must participate in the fusion.

The search presented here is performed under the simplifying assumption that one of the λ'_{1jk} dominates. The squarks decay either via their Yukawa coupling into SM fermions ($\not{R}_p$), or via their usual gauge couplings (gauge decay) into a gluino $\tilde{g}$ (the SUSY partner of the gluon), a neutralino χ^0_α ($\alpha = 1, 4$) or a chargino $\chi^\pm_\beta$ ($\beta = 1, 2$). The mass eigenstates χ^0_α are mixed states of the photino, the zino and the neutral higgsinos, which are the SUSY partners of the photon, of the Z and of the two neutral Higgs fields respectively. The charginos $\chi^\pm_\beta$ are mixed states of the charged higgsinos and of the winos, SUSY partners of the $W^\pm$. Neutralinos, charginos and gluinos are unstable. This holds in $\not{R}_p$ SUSY also for the Lightest Supersymmetric Particle (LSP), assumed here to be a χ (χ^0 or $\chi^\pm$) or a $\tilde{g}$, which decays into a quark, an antiquark and a lepton [5], via a virtual squark or slepton undergoing a $\not{R}_p$ decay through the λ' coupling. This is in contrast to R_p conserving SUSY models and has important phenomenological consequences.

In cases where both production and decay occur through a λ'_{1jk} coupling (e.g. Fig. 1a and c for $\lambda'_{1j1} \neq 0$), the squarks have the same signature as scalar leptoquarks (LQ) [6]. As can be seen from equation (1), the $\overline{\tilde{d}^k_R}$ can decay either into $e^+ + \bar{u}^j$ or $\bar{\nu}_e + \bar{d}^j$, while the $\tilde{u}^j_L$ only decays into $e^+ + d^k$. The final state signatures consist of a lepton and a jet and are, event-by-event, indistinguishable from SM neutral current (NC) and charged current (CC) Deep-Inelastic Scattering (DIS).

When the $\tilde{u}^j_L$ ($\overline{\tilde{d}^k_R}$) undergoes a gauge decay into a χ^0, a χ^+ or a $\tilde{g}$ (a χ^0 or a $\tilde{g}$) as shown in Fig. 1b and d, the final state will depend on their subsequent decays. Neutralinos χ^0_α with $\alpha > 1$ as well as charginos (gluinos) usually undergo gauge decays into a lighter χ and two SM fermions (two quarks), through a real or virtual boson or sfermion (squark). The decay chain ends with the $\not{R}_p$ decay of one sparticle, usually that of the LSP.

$\not{R}_p$ decays of χ's or gluinos are mainly relevant for the lightest states. Neutralinos can undergo the $\not{R}_p$ decays $\chi^0 \to e^\pm q\bar{q}'$ or $\chi^0 \to \nu q\bar{q}$, the former (latter) being more frequent if the χ^0 is dominated by its photino (zino) component. Gluinos can undergo the same $\not{R}_p$ decays. When a χ^0 or a $\tilde{g}$ decays via $\not{R}_p$ into a charged lepton, both the "right" and the "wrong" charge

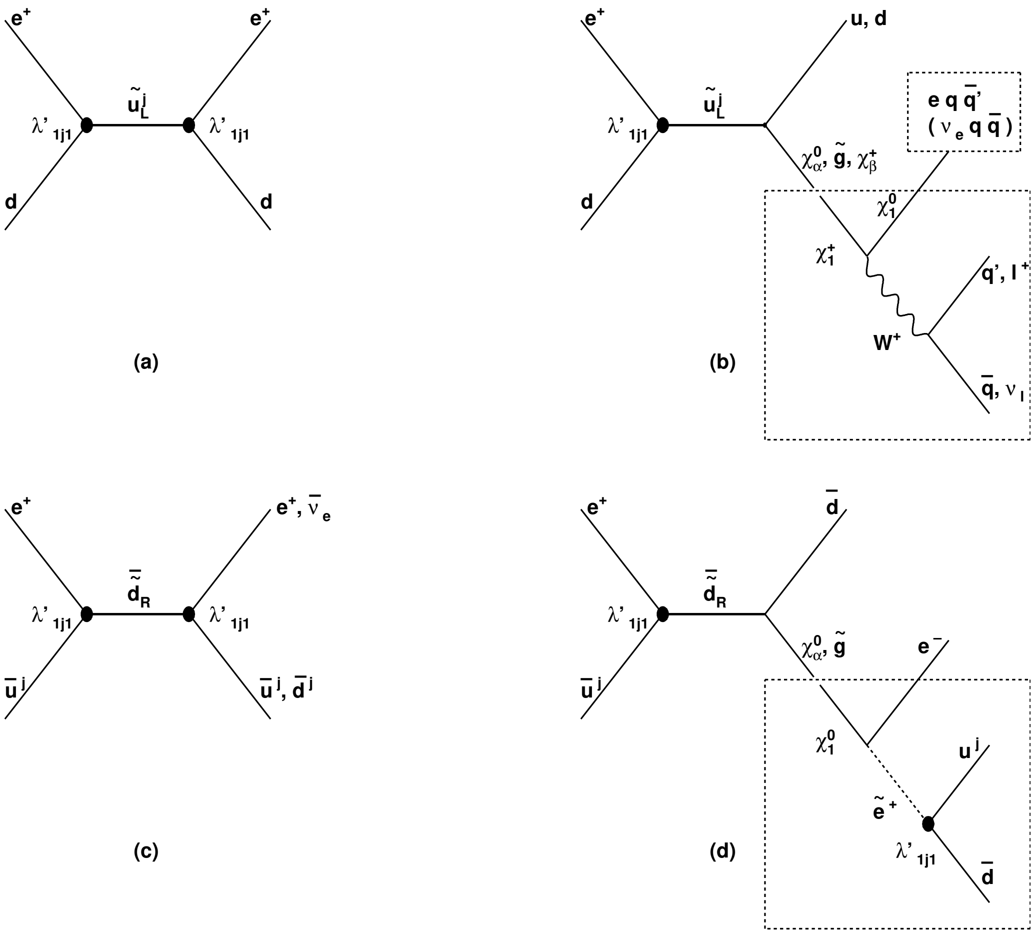

Figure 1: Lowest order s-channel diagrams for $\not\!\!R_p$ squark production at HERA followed by (a), (c) $\not\!\!R_p$ decays and (b), (d) gauge decays of the squark. In (b) and (d), the emerging neutralino, chargino or gluino might subsequently undergo a R_p violating or R_p conserving decay of which examples are shown in the dashed boxes for (b) the χ_1^+ and (d) the χ_1^0.

lepton (with respect to the incident beam) are equally probable, this latter case leading to largely background free striking signatures for lepton number violation. In contrast, the only possible $\not\!\!R_p$ decays for charginos are $\chi^+ \rightarrow \bar{\nu} u^k \bar{d}^j$ and $\chi^+ \rightarrow e^+ d^k \bar{d}^j$.

The decay chains of $\tilde{u}_L^j$ and $\overline{\tilde{d}_R^k}$ analysed in this paper are classified into seven distinguishable event topologies as described in table 2. This classification relies on the number of charged leptons and/or jets in the final state, and on the presence of missing energy. Channels labelled $\boldsymbol{LQe}$ and $\boldsymbol{LQ\nu}$ are the "leptoquark-like" decay modes of the squark, proceeding directly via $\not\!\!R_p$, while the remaining channels cover the gauge decays of the squark and are characterised by multijet (MJ) final states. Channels labelled $\boldsymbol{eMJ}$, $\boldsymbol{e^-MJ}$ and $\boldsymbol{\nu MJ}$ involve one or two SUSY fermions (χ or $\tilde{g}$) denoted by X and Y in table 2. Channels $\boldsymbol{e\ell MJ}$ and $\boldsymbol{\nu\ell MJ}$ necessarily involve two SUSY fermions. Decay patterns involving more than two χ or $\tilde{g}$ are kinematically suppressed and are not searched for explicitly. The relative contributions of the channels considered depend in particular on the value of the Yukawa coupling λ' and on the gaugino[2]-higgsino mixture of neutralinos and charginos. They will be shown as functions of the squark mass in section 6.2 for some example cases.

[2]The gauginos are the SUSY partners of the gauge bosons.

Additional event topologies not listed in table 2 could in principle arise in the case where the χ_1^0 has such a small decay width (e.g. when it has large higgsino components) that it decays far away from the interaction point or leads to final states with displaced vertices [2]. However the region of MSSM parameter space which would allow a χ^0 to escape detection for a finite value of the $\not{R}_p$ coupling is now very severely constrained by the searches for charginos carried out at LEP [7, 8]. The lifetimes of the sparticles are neglected in this analysis.

3 The H1 Detector

A detailed description of the H1 detector can be found in [9]. Here we describe only the components relevant for the present analysis in which the final state of the events involves either a positron[3] with high transverse energy or a large amount of hadronic transverse energy flow.

The positron energy and angle are measured in a liquid argon (LAr) sampling calorimeter [10] covering the polar angular range 4° $\leq \theta \leq$ 154° and all azimuthal angles. Polar angles are defined by taking the origin of the coordinate system to be at the nominal interaction point and the z-axis in the direction of the proton beam. The granularity of the LAr calorimeter is optimised to provide fine and approximately uniform segmentation in laboratory pseudorapidity η and azimuthal angle ϕ. The calorimeter consists of a lead/argon electromagnetic section followed by a stainless steel/argon hadronic section. Test beam measurements [11] of the LAr calorimeter modules have shown an energy resolution of $\sigma(E)/E \simeq 12\%/\sqrt{E/\text{ GeV}} \oplus 1\%$ for electrons and $\sigma(E)/E \simeq 50\%/\sqrt{E/\text{ GeV}} \oplus 2\%$ for pions. The angular resolution on the positron measured from the electromagnetic shower in the calorimeter varies from ~ 2 mrad below 30° to $\lesssim 5$ mrad at larger angles. For the acquisition of events we rely on the LAr trigger system [10] whose efficiency is close to 100% for the transverse energies (E_T) considered here. A lead/scintillating-fibre backward calorimeter [12] extends the coverage[4] at larger angles (153° $\leq \theta \lesssim$ 178°).

The tracking system which is surrounded by the calorimeters is used in particular to determine the position of the interaction vertex. The main components of this system are central drift and proportional chambers (25° $\leq \theta \leq$ 155°), a forward track detector (7° $\leq \theta \leq$ 25°) and a backward drift chamber. The tracking chambers and calorimeters are surrounded by a superconducting solenoid providing a uniform field of 1.15 T parallel to the z axis within the detector volume. The instrumented iron return yoke surrounding this solenoid is used to measure leakage of hadronic showers and to recognise muons. In the very forward region ($\theta \leq 15°$) muons can also be detected in three double layers of drift chambers, forming the Forward Muon Detector. The luminosity is determined from the rate of Bethe-Heitler $ep \rightarrow ep\gamma$ bremsstrahlung events measured in a luminosity monitor.

4 Monte Carlo Event Generation

For each possible SM background source, complete Monte Carlo simulations of the H1 detector response are performed. Most of them correspond to a luminosity of more than 10 times that of the data.

[3] Unless otherwise stated, the analysis does not distinguish explicitly between e^+ and e^-.

[4] The detectors in the backward region were upgraded in 1995 by the replacement of the lead/scintillator tile calorimeter [13] and a proportional chamber.

Channel	Decay processes	Signature
$\boldsymbol{LQe}$	$\tilde{q} \xrightarrow{\lambda'} e^+ \quad q$	high P_T e^+ + 1 jet
$\boldsymbol{LQ\nu}$	$\overline{\tilde{d}^k_R} \xrightarrow{\lambda'} \bar{\nu}_e \quad \bar{d}$	missing P_T + 1 jet
$\boldsymbol{eMJ}$	$\tilde{q} \longrightarrow q \quad X$ $\overset{\lambda'}{\hookrightarrow} \; e^+\bar{q}q$ $\tilde{q} \longrightarrow q \quad X$ $\hookrightarrow \; q\bar{q} \quad Y$ $\overset{\lambda'}{\hookrightarrow} e^+\bar{q}q$	e^+ + multiple jets
$\boldsymbol{e^-MJ}$	$\tilde{q} \longrightarrow q \quad \chi^0_\alpha, \tilde{g}$ $\overset{\lambda'}{\hookrightarrow} \; e^-\bar{q}q$ $\tilde{q} \longrightarrow q \quad X$ $\hookrightarrow \; q\bar{q} \quad Y$ $\overset{\lambda'}{\hookrightarrow} e^-\bar{q}q$	e^- (i.e. wrong sign lepton) + multiple jets
$\boldsymbol{\nu MJ}$	$\tilde{q} \longrightarrow q \quad X$ $\overset{\lambda'}{\hookrightarrow} \; \nu\bar{q}q$ $\tilde{q} \longrightarrow q \quad X$ $\hookrightarrow \; q\bar{q} \; Y$ $\overset{\lambda'}{\hookrightarrow} \nu\bar{q}q'$	missing P_T + multiple jets
$\boldsymbol{e\ell MJ}$	$\tilde{q} \longrightarrow q \quad X$ $\hookrightarrow \; \ell\nu_\ell \quad Y$ $\overset{\lambda'}{\hookrightarrow} e^\pm\bar{q}q$ $\tilde{q} \longrightarrow q \quad X$ $\hookrightarrow \; \ell^+\ell^- \quad Y$ $\overset{\lambda'}{\hookrightarrow} e^\pm\bar{q}q$ $\tilde{q} \longrightarrow q \quad X$ $\hookrightarrow \; e^+e^- \quad Y$ $\overset{\lambda'}{\hookrightarrow} \nu\bar{q}q$	e + ℓ (e or μ) + multiple jets
$\boldsymbol{\nu\ell MJ}$	$\tilde{q} \longrightarrow q \quad X$ $\hookrightarrow \; \ell\nu_\ell \quad Y$ $\overset{\lambda'}{\hookrightarrow} \nu\bar{q}q$ $\tilde{q} \longrightarrow q \quad X$ $\hookrightarrow \; \mu^+\mu^- \quad Y$ $\overset{\lambda'}{\hookrightarrow} \nu\bar{q}q$	ℓ (e or μ) + missing P_T + multiple jets

Table 2: Squark decay channels in $R\!\!\!/_p$ SUSY classified by distinguishable event topologies. X and Y denote a neutralino, a chargino or a gluino. Quarks are generically denoted by q, except for the $\boldsymbol{LQ\nu}$ channel which involves specific (s)quark flavours. The final states corresponding to $\ell = \tau$ for the $\boldsymbol{e\ell MJ}$ and $\boldsymbol{\nu\ell MJ}$ channels are not explicitly looked for in this analysis.

For the simulation of the NC and CC DIS backgrounds, the DJANGO [14] event generator is used, which includes first order QED radiative corrections. QCD radiation is treated following the approach of the Colour Dipole Model [15] and is implemented using ARIADNE [16]. The hadronic final state is generated using the string fragmentation model [17]. The parton densities in the proton used to estimate DIS expectations are taken from the MRST [18] parametrisation.

For direct and resolved photoproduction (γp) of light and heavy flavours, the PYTHIA event generator [19] is used which relies on first order QCD matrix elements and uses leading-log parton showers and string fragmentation [17]. The GRV (GRV-G) parton densities [20] in the proton (photon) are used.

The simulation of the leptoquark-like signatures ($\boldsymbol{LQe}$ and $\boldsymbol{LQ\nu}$) relies on the event generator LEGO [21] which is described in more detail in [3, 22]. For squarks undergoing gauge decays, we use the SUSYGEN [23] event generator, recently extended [24] to allow the generation of SUSY events in ep collisions. Any gauge decay of the squark can be generated, and the cascade decays of the subsequent χ's or $\tilde{g}$ are performed according to the corresponding matrix elements.

In both LEGO and SUSYGEN, initial and final state parton showers are simulated following the DGLAP [25] evolution equations, and string fragmentation [19, 17] is used for the non-perturbative part of the hadronisation. In addition initial state bremsstrahlung in the collinear approximation is simulated in the LEGO generator. The parton densities used [18] are evaluated at the scale of the squark mass. This scale is also chosen for the maximum virtuality of parton showers initiated by a quark coming from the squark decay. Moreover, in the SUSYGEN generator, the parton showers modelling QCD radiation off quarks emerging from a χ or $\tilde{g}$ decay are started at a scale given by the mass of this sparticle.

To allow a model independent interpretation of the results, the signal topologies given in table 2 were simulated for a wide range of masses of the SUSY particles. The events were passed through a complete simulation of the H1 detector. The squark mass was varied from 75 GeV to 275 GeV in steps of typically 25 GeV. Gauge decays of squarks involving one or two SUSY fermions (χ or $\tilde{g}$) were simulated separately. For gauge decays of squarks into a χ^0, a χ^+ or a $\tilde{g}$ which directly decays via $\not{R}_p$ (i.e. processes corresponding to the first line of the $\boldsymbol{eMJ}$, $\boldsymbol{e^-MJ}$ and $\boldsymbol{\nu MJ}$ rows in table 2) the process $\tilde{q} \to q\chi_1^0$ was simulated for χ_1^0 masses ranging between 40 GeV and 160 GeV. In order to study gauge decays involving two χ or $\tilde{g}$, the process $\tilde{q} \to q\chi_1^+ \to q\chi_1^0 f\bar{f}'$ was simulated for χ_1^+ masses ranging between 90 GeV and $\sim M_{\tilde{q}}$, and for χ_1^0 masses between half of the χ_1^+ mass and $\sim M_{\chi_1^+}$. Masses of the χ's were varied in steps of about 20 GeV. These simulations allowed the determination of signal selection efficiencies as a function of the masses of the squark and of the involved χ or $\tilde{g}$ for essentially all allowed scenarios, since the grid size chosen for the simulated scenarios was small enough for a linear interpolation between them.

5 Event Selection and Comparison with Standard Model Expectation

The data reduction starts by the rejection of non-ep background, which is common to all channels presented below. It is required that the events are accepted by a set of beam halo and cosmic muon filters [26], that they satisfy constraints on their timing relative to the nominal time of the beam bunch crossings, and that a primary interaction vertex is reconstructed.

Events containing lepton(s), hard jets, or a large amount of missing transverse energy are then selected using the following identification criteria:

- a **positron** (or electron) is identified by a shower shape analysis of clustered energy deposits in the LAr calorimeter; the positron energy cluster should contain more than 98% of the LAr energy found within a pseudorapidity-azimuthal cone centered around the positron direction and of opening $\sqrt{(\Delta\eta)^2 + (\Delta\phi)^2} = 0.25$, where $\eta = -\ln\tan\frac{\theta}{2}$; at least one charged track is required within this isolation cone;

- a **muon** candidate is identified as a track measured in the central and/or forward tracking system, which has to match geometrically an energy deposit in the LAr calorimeter compatible with a minimum ionising particle, and/or a track in the instrumented iron and/or a track in the forward muon detector;

- **hadronic jets** are reconstructed from energy deposits in the LAr calorimeter using a cone algorithm in the laboratory frame with a radius $\sqrt{\Delta\eta^2 + \Delta\phi^2} = 1$; the fraction of the jet energy deposited in the hadronic part of the calorimeter must be at least 5%;

- the **missing transverse momentum** $P_{T,miss}$ is obtained as

$$P_{T,miss} \equiv \sqrt{\left(\sum E_i \sin\theta_i \cos\phi_i\right)^2 + \left(\sum E_i \sin\theta_i \sin\phi_i\right)^2} \tag{2}$$

  where the summation runs over all energy deposits i in the calorimeters.

In addition, the selection makes use of the following kinematic variables:

- the momentum balance with respect to the direction of the incident positron, obtained as:

$$\sum (E - P_z) \equiv \sum E_i \, (1 - \cos\theta_i) \tag{3}$$

  where the summation runs over all energy deposits i in the calorimeters. $\sum (E - P_z)$ should peak at twice the energy E_e^0 of the incident positron for events where only particles escaping in the proton direction remain undetected;

- the Lorentz invariants y, Q^2 and x characterising the kinematics of a DIS reaction, as well as the energy M in the centre of mass of the hard subprocess, are determined using the measurement of the polar angle θ_e, the energy E_e and the transverse energy $E_{T,e}$ of the highest E_T positron:

$$y_e = 1 - \frac{E_e(1 - \cos\theta_e)}{2E_e^0}, \quad Q_e^2 = \frac{E_{T,e}^2}{1 - y_e}, \quad x_e = \frac{Q_e^2}{y_e s}, \quad M_e = \sqrt{x_e s} \;\; ;$$

- the variables y, Q^2, x and M calculated using the Jacquet-Blondel ansatz [27]:

$$y_h = \frac{\sum (E - P_z)_h}{2E_e^0}, \quad Q_h^2 = \frac{P_{T,h}^2}{1 - y_h}, \quad x_h = \frac{Q_h^2}{y_h s}, \quad M_h = \sqrt{x_h s} \;\; ;$$

  where $P_{T,h}$ and $\sum (E - P_z)_h$ are calculated as in equations (2) and (3), but restricting the summations to all measured hadronic final state energy deposits.

The search for squarks decaying via $\not{R}_p$ couplings into channels $\boldsymbol{LQe}$ and $\boldsymbol{LQ\nu}$ is identical to the search for first generation leptoquarks presented in [1]. Gauge decay channels are grouped into two classes, $e +$ jets $+ X$ and $\nu +$ jets $+ X$. Preselection criteria are designed for these two classes of events, on top of which dedicated cuts are applied for the gauge decay channels listed in table 2. For all considered channels, the selection criteria are given in table 3 together with the resulting signal efficiencies and the numbers of observed and expected events.

5.1 Analysis of Squark R-Parity Violating Decays

Channel LQe: Squarks decaying into the channel LQe have the same signature as scalar leptoquarks and are characterised by high Q^2 NC DIS-like topologies. Such a process should manifest itself as a resonance in the measured M_e distribution, with a resolution of 3 to 6 GeV depending on the squark mass. The selection criteria are those described in [1]. The observed and expected mass spectra are shown in Fig. 2a to be in good agreement, with nevertheless a slight excess around 200 GeV already reported in [1, 28]. The sources of systematic errors are described in section 5.4. The (arbitrarily normalised) mass distribution expected from signal events coming from a 200 GeV squark decaying into the channel LQe is also shown. The peak value is slightly below the nominal squark mass due to final state QCD radiation [1]. Similar searches have been performed by the ZEUS experiment [29].

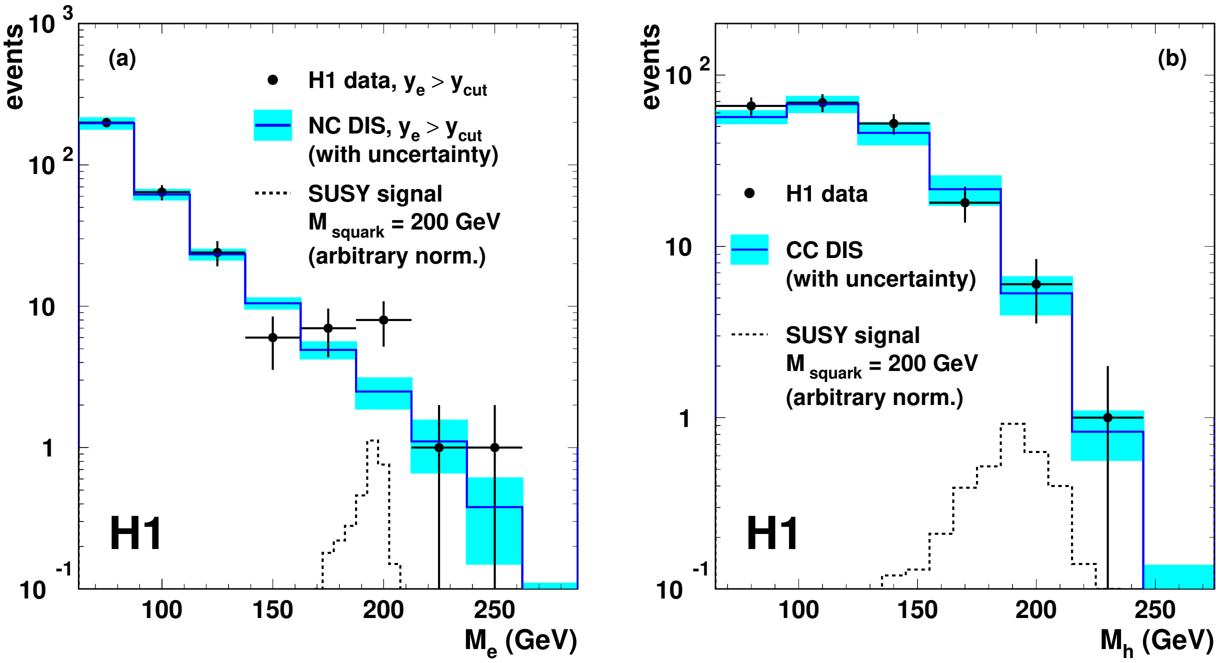

Figure 2: Mass spectra for (a) NC DIS-like and (b) CC DIS-like final states for data (symbols) and DIS expectation (solid histograms). In (a) the comparison is shown after a M_e dependent cut on y_e designed to maximise the significance of a squark signal [1]. The grey boxes indicate the $\pm 1\sigma$ band of systematic errors of the DIS expectations. The dashed histograms show the mass distributions for simulated events coming from a 200 GeV squark decaying into the channels (a) LQe and (b) $LQ\nu$, with an arbitrary normalisation.

Channel $LQ\nu$: Squarks undergoing a $LQ\nu$ decay lead to CC DIS-like events with high missing transverse momentum showing a clustering in the M_h distribution with a resolution of about 10% of the squark mass. Only $\overline{\tilde{d}_R^k}$ squarks, produced via a fusion between the incident e^+ and a $\bar{u}^j$ quark can undergo such a decay. The search for squarks decaying into the channel $LQ\nu$ is described in [1]. The observed and expected mass spectra are shown to be in good agreement in Fig. 2b. The (arbitrarily normalised) mass distribution expected from signal events coming from a 200 GeV squark decaying into the channel $LQ\nu$ is also shown. Similar searches have been performed by the ZEUS experiment [30].

5.2 Analysis of Squark Gauge Decays leading to e + jets + X Topologies

When the squark undergoes a gauge decay leading to a positron, the final states can be classified into several topologies, namely $\boldsymbol{eMJ}$, $\boldsymbol{e^-MJ}$, $\boldsymbol{eeMJ}$, $\boldsymbol{e\mu MJ}$ and $\boldsymbol{\nu eMJ}$. The "e-preselection" requirements which are common to all these e + multijet channels are the following:

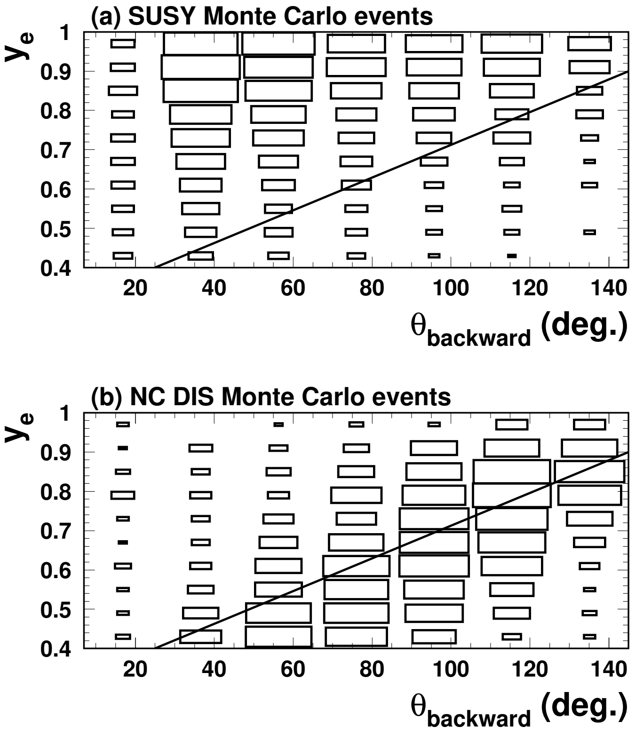

Figure 3: Correlation between y_e and the angle of the most backward jet, $\theta_{backward}$, for (a) SUSY Monte Carlo events where the squark undergoes a gauge decay leading to e + multijets $+X$ final states and (b) NC DIS Monte Carlo events, when preselection cuts (1) to (3) are applied. Cut (4) only retains events above the diagonal line. In (a) events were generated for the range of masses considered in this analysis.

1. at least one positron candidate in the angular range $5° < \theta_e < 110°$ with $E_{T,e} > 5$ GeV;
2. at least two jets in the angular range $7° < \theta < 145°$; the highest E_T jet must satisfy $\theta_{jet\,1} > 10°$ and $E_{T,jet\,1} > 15$ GeV; the second highest E_T jet must have $E_{T,jet\,2} > 10$ GeV;
3. $y_e > 0.4$;
4. of the two highest E_T jets, the one with the larger polar angle, $\theta_{backward}$, must satisfy:
$$y_e - 0.4 > (\theta_{backward} - 25°)/60°;$$
5. the minimum of the polar angles of the highest E_T positron and of the two highest E_T jets must satisfy:
$$\mathrm{Min}(\theta_\mathrm{e}, \theta_{\mathrm{jet}\,1}, \theta_{\mathrm{jet}\,2}) < 45° \quad .$$

In gauge decays of a squark, a positron can emerge from the decay of a χ or $\tilde{g}$ appearing in the decay chain. It takes away a (possibly small) fraction of the momentum of this fermion, which motivates the cut (3). Moreover, it is strongly boosted in the direction of the incident proton, such that the $\theta_e < 110°$ requirement discriminates the signal from the NC DIS background. Cut (4) exploits the fact that for high y_e NC DIS events satisfying the above set of cuts, one hard jet is usually scattered in the backward region of the calorimeter. In contrast, jets coming from a squark gauge decay will be boosted in the forward direction. The $\theta_{backward}$ distribution for SUSY events depends on the masses of the sparticles involved and cut (4) was designed to always retain a large fraction of the signal events. The effect of cut (4) is illustrated in Fig. 3. Cut (5) requires that one of the squark decay products should be emitted in the forward direction and allows an additional reduction of the SM background by $\sim 40\%$, with a negligible efficiency loss on the signal.

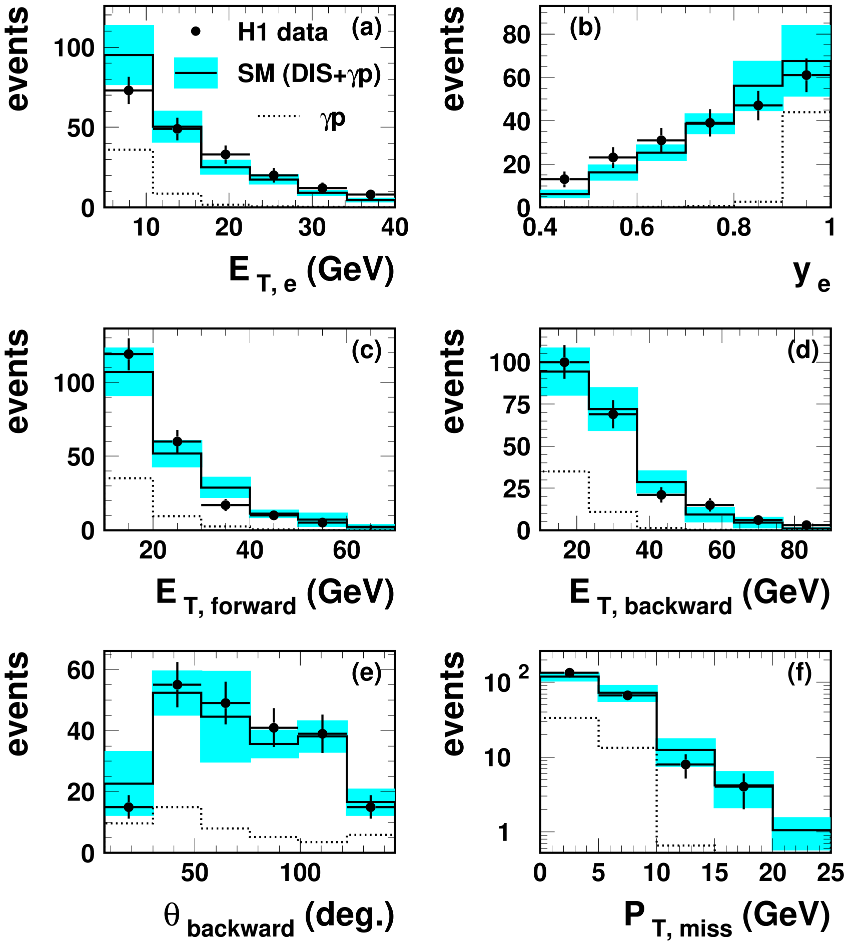

Figure 4: For the e + multijets $+X$ preselection, distributions of (a) the transverse energy $E_{T,e}$ of the highest E_T positron; (b) y_e; (c) the transverse energy of the most forward jet; (d) the transverse energy of the most backward jet; (e) the polar angle of the most backward jet; (f) the missing transverse momentum. Superimposed on the data points (symbols) are histograms of the SM expectation (DIS and γp). The grey band indicates the uncertainty on the SM prediction. The contribution from γp processes alone is shown as dotted histograms.

Applying the above selection criteria, 214 events are accepted, which is in good agreement with the SM prediction of 210 ± 34, including 47 events from photoproduction where a jet has been misidentified as an electron. Fig. 4 shows the observed distributions of the transverse energy of the highest E_T positron, y_e, the transverse energy of the most forward and most backward jet, the polar angle of the most backward jet and the missing transverse momentum.

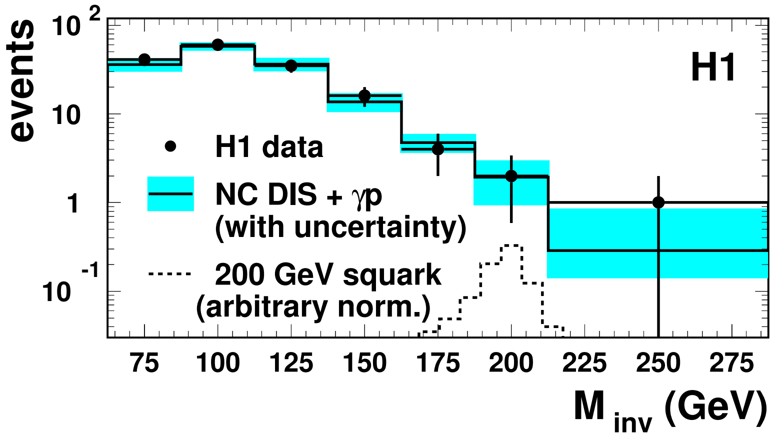

Figure 5: Mass spectrum for e + multijet topology $\boldsymbol{eMJ}$ for the data (symbols) and the SM expectation (solid histogram). The grey band indicates the uncertainty on the SM prediction. The dashed histogram shows the expected mass distribution for events coming from a 200 GeV squark decaying into the channel $\boldsymbol{eMJ}$, with an arbitrary normalisation.

All distributions are seen to agree well with the SM expectation within the systematic errors.

For channels leading to $e+$ jets $+X$ final states additional cuts, listed in table 3, are applied on top of the preselection requirements (1) to (5). In each case, good agreement is observed between the data and the SM expectation largely dominated by the NC DIS contribution. Additional information for the different channels is given below.

Channel $\boldsymbol{eMJ}$: A mass M_{inv} is calculated as:

$$M_{inv} = \sqrt{4x_e E_e^0 \left(\sum_i E_i - E_e^0 \right)} \ ,$$

where the sum runs over all energy deposits in the calorimeters for $\theta > 10°$, thereby excluding the proton remnant. For squarks decaying into the $\boldsymbol{eMJ}$ channel, M_{inv} provides an estimate of the $\tilde{q}$ mass. This reconstruction method yields a typical resolution of 7 to 10 GeV depending on the squark mass. The M_{inv} spectrum of the selected events is shown in Fig. 5 to be well described by the SM prediction. Also shown is the (arbitrarily normalised) mass distribution expected from signal events coming from a 200 GeV squark decaying into the channel $\boldsymbol{eMJ}$. No charge determination of the lepton is performed here.

Channel $\boldsymbol{e^-MJ}$: We consider the track in the e isolation cone which has the highest momentum projected on the axis defined by the event vertex and the centre of gravity of the calorimetric energy deposits associated with the electron. This track is required to have a reliably measured negative charge. The efficiency of the track quality requirements is $\simeq 80\%$, derived from data (candidates for channel $\boldsymbol{eMJ}$) and well reproduced by the NC DIS simulation.

Channel $\boldsymbol{e\ell MJ}$: Di-lepton final states are searched for provided that the lepton accompanying the e belongs to the first or second generation. For the channel $\boldsymbol{e\mu MJ}$, the properties of the muons observed in the preselected events over the full range in transverse momentum were found to be well described by the simulation, as exemplified in Fig. 6.

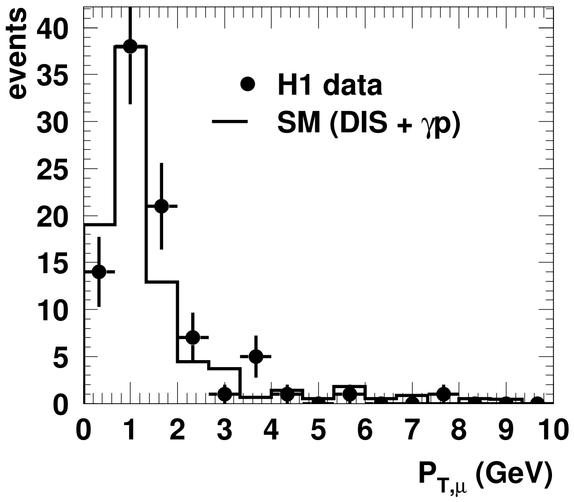

Figure 6: Distribution of the transverse momentum $P_{T,\mu}$ of the muon for events satisfying the preselection criteria and where a muon has been identified in the angular range $10^\circ < \theta < 110^\circ$, for data (points) and SM (histogram).

Channel $\boldsymbol{\nu eMJ}$: The common preselection criteria are complemented by a $P_{T,miss}$ requirement and by the cut $y_e \cdot (y_e - y_h) > 0.05$. A cut on the product of y_e with the difference $(y_e - y_h)$ exploits the fact that, for events coming from a squark decaying into the channel $\boldsymbol{\nu eMJ}$, the escaping neutrino carries a non-negligible part of $\sum (E - P_z)$ and hence the variable y_h is substantially smaller than y_e, while $y_e \sim y_h$ is expected for NC DIS events. Fig. 7 shows the distribution of $y_e \cdot (y_e - y_h)$ for the 214 events accepted by the preselection and for the SM expectation.

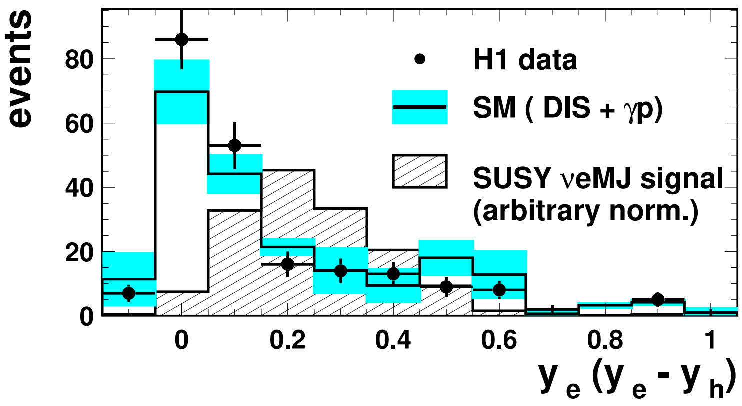

Figure 7: Distribution of the variable $y_e \cdot (y_e - y_h)$ for the 214 events satisfying the preselection criteria (symbols) and for the expectation from NC DIS and γp processes (open histogram). The grey error band on the open histogram indicates the uncertainty on the SM prediction. The arbitrarily normalised hatched histogram shows how this variable is distributed for events coming from a squark decaying into the channel $\boldsymbol{\nu eMJ}$, generated for the range of masses considered in this analysis.

5.3 Analysis of Squark Gauge Decays leading to ν + jets + X Topologies

Two channels are considered to cover cases where squarks undergo a gauge decay leading to a neutrino (and no positron) in the final state. These final states, $\boldsymbol{\nu MJ}$ and $\boldsymbol{\nu\mu MJ}$, are selected by the following "ν-preselection" requirements:

1. a missing transverse momentum $P_{T,miss} > 25$ GeV;
2. at least two jets in the angular range $7° < \theta < 145°$ and with $E_T > 10$ GeV, with the highest E_T jet satisfying $\theta_{jet\,1} > 10°$ and $E_{T,\,jet\,1} > 15$ GeV.

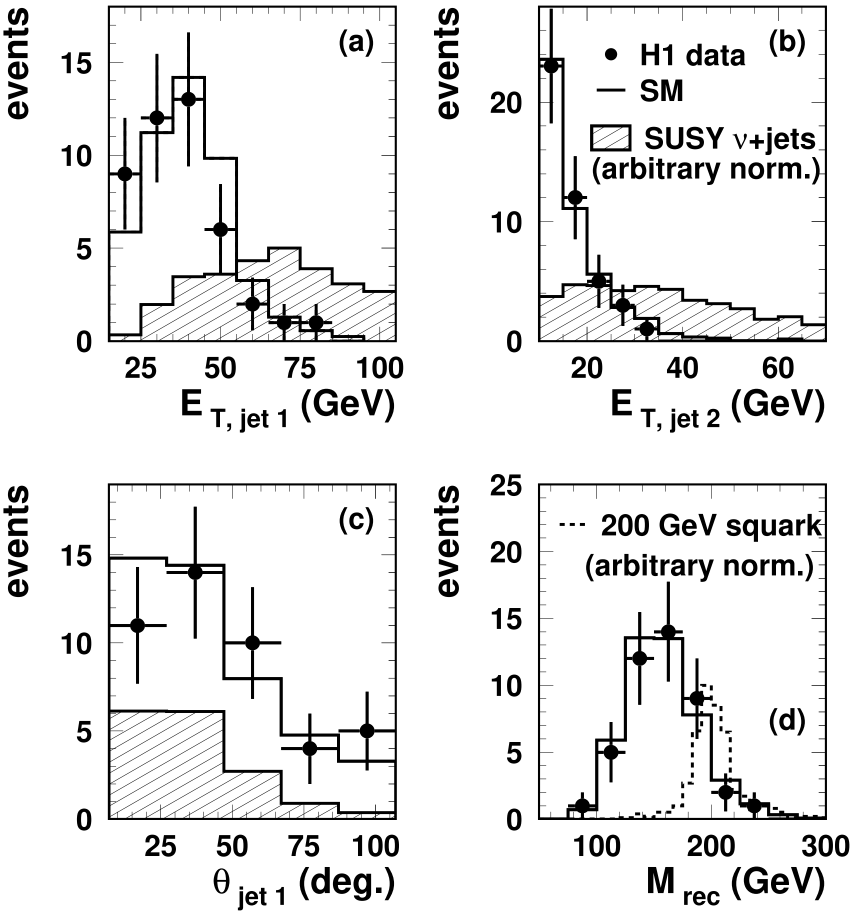

Figure 8: For the ν + multijets $+X$ preselection, observed (symbols) and expected (open histograms) distributions of (a), (b) the transverse energies of the two highest E_T jets and (c) the polar angle of the highest E_T jet. The hatched histograms show distributions for events from a squark gauge decay into ν + jets, generated for the range of masses considered in this analysis. (d): The mass M_{rec}, corresponding to the energy in the centre of mass of the hard subprocess assuming that only one neutrino escapes detection; the dashed histogram shows the M_{rec} distribution for signal events coming from the decay of a 200 GeV squark into the channel $\boldsymbol{\nu MJ}$. All histograms showing the SUSY expectation are arbitrarily normalised.

We observe 44 events satisfying these preselection criteria, in good agreement with the SM prediction of 46.5 ± 6.9, mainly coming from CC DIS processes.

Figs. 8a-c show the distributions of the transverse energies of the two highest E_T jets and of the polar angle of the highest E_T jet. The data are well described by the SM expectation. Distributions for squarks decaying into ν + jets are also shown. Assuming that the missing energy is carried by one neutrino only, its kinematics is reconstructed exploiting energy-momentum conservation. The four-vector of this ν is then added to that of the hadronic final state to reconstruct the invariant mass M_{rec} of the incoming electron and quark. For squarks decaying into the channel $\boldsymbol{\nu MJ}$, M_{rec} provides an estimate of the squark mass. The observed and expected distributions for M_{rec} are in good agreement as shown in Fig. 8d. The dashed, arbitrarily normalised, histogram in Fig. 8d shows the resulting mass spectrum for a 200 GeV squark decay into the $\boldsymbol{\nu MJ}$ channel. The observed resolution of ~ 15 GeV is typical for the range of squark masses probed in this analysis.

Final cuts and results for the channels $\boldsymbol{\nu MJ}$ and $\boldsymbol{\nu\mu MJ}$ are given in table 3. The number of observed candidates is in good agreement with the SM expectation, which is dominated by the contribution of CC DIS processes.

5.4 Systematic Errors

In each channel, the error on the expectation from Standard Model processes has been calculated by taking into account the systematic errors described below. The experimental error sources considered are:

- an uncertainty of $\pm 1.5\%$ on the integrated luminosity;
- an uncertainty on the absolute calibration of the calorimeters for electromagnetic energies, ranging between $\pm 0.7\%$ in the central part and $\pm 3\%$ in the forward region of the LAr calorimeter; this constitutes the main error source for the estimation of NC DIS background to the channel $\boldsymbol{LQe}$;
- an uncertainty of $\pm 4\%$ on the absolute hadronic energy scale. For inclusive NC DIS final states, the over-constrained kinematics allows a reduction of this uncertainty to $\pm 2\%$ [26], which applies to channels $\boldsymbol{LQe}$ and $\boldsymbol{LQ\nu}$. This is the main error source for all channels except $\boldsymbol{LQe}$.

The following theoretical uncertainties on SM cross-sections are considered.

- For NC DIS-like final states, an uncertainty of $\pm 5\%$ is attributed to the proton structure [28], which is partly due to the experimental errors on the input data entering the QCD fits, and partly linked to the assumptions for the shapes of the parton distributions at the scale where the perturbative QCD evolution is started. For CC DIS-like topologies, which are mainly induced by d quarks whose density in the proton is less constrained, this uncertainty increases linearly with Q^2 up to $\simeq 20\%$ at the highest Q^2 considered here [1]. In adition, the error on the strong coupling constant α_S leads to an uncertainty of $\pm 4\%$ on the proton structure. This was inferred [28] by comparing the CTEQ4 (A1) to (A5) parametrisations [31] with $\alpha_S(M_Z)$ ranging between 0.110 to 0.122.

Channel	Selection Cuts	Efficiency	N_{obs}	N_{exp}
DIS-like channels: $Q^2 > 2500$ GeV^2, $y < 0.9$				
$\boldsymbol{LQe}$	$E_{T,e} > 15$ GeV $P_{T,miss}/\sqrt{E_{T,e}} \leq 4\sqrt{\text{GeV}}$ $40 \leq \sum(E-P_z) \leq 70$ GeV optimised lower y-cut	40–70 %	310	301 ± 23
$\boldsymbol{LQ\nu}$	$P_{T,miss} > 30$ GeV no electron $E_{T,e} > 5$ GeV	30–80 %	213	199 ± 12
channels with: e **+ multijets + X** e-preselection: $E_{T,e} > 5$ GeV; $\geq$ 2 jets: $E_{T,jet\,1,2} > 15, 10$ GeV; high y_e; angular cuts				
$\boldsymbol{eMJ}$	$P_{T,miss} < 20$ GeV $40 \leq \sum(E-P_z) \leq 70$ GeV	35–50 %	159	151 ± 17
$\boldsymbol{e^-MJ}$	eMJ criteria + “wrong” charge of e	$\approx 30\%$	0	1.3 ± 0.5
$\boldsymbol{eeMJ}$	second e with: $E_{T,e2} > 5$ GeV $5° < \theta_{e2} < 110°$	$\approx 30\%$	0	0.7 ± 0.4
$\boldsymbol{e\mu MJ}$	$P_{T,\mu} > 5$ GeV $10° < \theta_\mu < 110°$	35–50%	2	4.2 ± 1.2
$\boldsymbol{\nu eMJ}$	$P_{T,miss} > 15$ GeV $y_e(y_e - y_h) > 0.05$	$\approx 30\%$	1	3.2 ± 1.2
channels with: ν **+ multijets + X** ν-preselection: $P_{T,miss} > 25$ GeV; $\geq$ 2 jets: $E_{T,jet\,1,2} > 15, 10$ GeV				
$\boldsymbol{\nu MJ}$	$E_{T,jet2} > 15$ GeV $\sum(E-P_z)_h < 55$ GeV	20–60 %	21	23 ± 4
$\boldsymbol{\nu\mu MJ}$	$P_{T,\mu} > 5$ GeV $10° < \theta_\mu < 110°$	$\approx 40\%$	0	0.5 ± 0.2

Table 3: Selection criteria, typical efficiencies, total number of observed events N_{obs} and the corresponding SM expectation N_{exp} with its uncertainty, for each squark decay channel analysed. The “e-preselection” criteria are detailed in section 5.2.

- Higher order QED corrections imply a $\pm 2\%$ uncertainty in the y range considered here [28], estimated using the HECTOR [32] program.
- An uncertainty of $\pm 10\%$ on the predicted cross-section for multijet final states is estimated by comparing leading order (LO) Monte Carlo simulations where higher order QCD radiation is modelled by either the dipole model or DGLAP parton showers, and next-to-leading order (NLO) calculations.

For each error source, the analysis has been repeated shifting the central value by ± 1 standard deviation to estimate their individual contribution. The overall systematic error on SM expectations is then determined as the quadratic sum of these individual errors and the statistical uncertainty on the Monte Carlo simulation.

6 Constraints on SUSY Models

No significant deviation from SM expectations has been found in the analysis of various $\not{R}_p$ and gauge decay channels. These channels are combined to set constraints on $\not{R}_p$ SUSY models.

As mentioned in section 2, when HERA operates with incident positrons, the best probed $\not{R}_p$ couplings are λ'_{1j1}, on which we mainly concentrate here. Such a coupling allows for the production of $\tilde{u}_L^j$ or $\overline{\tilde{d}_R^k}$ squarks, the latter with a much reduced rate due to the smaller parton density. Thus only $\tilde{u}_L^j$ production is considered. Since this squark does not decay into $\nu + q$ the channel $\boldsymbol{LQ\nu}$ is not taken into account in the derivation of limits. The $\tilde{s}_R$ production is also (conservatively) neglected when setting limits on λ'_{1j2}.

In this section, mass dependent upper limits on the Yukawa couplings are first derived in a "phenomenological" version of the MSSM where the masses of the sfermions are not related to the SUSY soft-breaking mass terms of the gauginos. Scans are then performed in the framework of this "phenomenological" MSSM as well as in the constrained MSSM, and bounds on the Yukawa couplings are set in these models. Results are finally interpreted in the framework of the minimal Supergravity model.

6.1 Derivation of Limits

Mass dependent upper limits on the production cross-section $\sigma(e^+p \rightarrow \tilde{u}_L^j)$ are obtained assuming Poisson distributions for the SM background expectations as well as for the signal. A standard Bayesian prescription with a flat prior probability density for the signal cross-section is used. Both systematic and statistical errors have been folded in channel by channel as described in [3]. Each channel contributes in the derivation of the limits via its branching ratio, the number of observed and expected events satisfying the relevant selection cuts and the corresponding selection efficiency. For the channels $\boldsymbol{LQe}$, $\boldsymbol{eMJ}$ and $\boldsymbol{\nu MJ}$, the numbers of observed and expected events are integrated within a mass bin which slides over the accessible mass range. The width of the mass bin is adapted to the expected mass resolution in each channel, such that this bin contains approximately 68% of the signal at a given squark mass. For the channels $\boldsymbol{e^-MJ}$, $\boldsymbol{e\ell MJ}$ and $\boldsymbol{\nu\ell MJ}$, where both the SM expectation and the observation are small, no mass restriction is imposed.

Events which fulfil the selection requirements of more than one channel are only counted as squark candidates in the channel with the highest sensitivity. This prescription is illustrated in table 4. Note that the potential overlap between channels $\boldsymbol{LQe}$ and $\boldsymbol{eMJ}$ is already considerably reduced by the mass bin requirements, since the corresponding reconstructed squark masses, M_e and M_{inv} respectively, differ by typically more than 20 GeV. The relative efficiency loss on the SUSY signal induced by this slight tightening of the cuts depends on the masses of the sparticles involved, and is found to vary between $\sim 0.5\%$ and $\sim 3\%$.

candidates fulfilling the selection criteria for channels:	are not considered in channel:
$\boldsymbol{eMJ}$ $\boldsymbol{e^-MJ}$ $\boldsymbol{eeMJ}$ $\boldsymbol{e\mu MJ}$ $\boldsymbol{\nu eMJ}$	$\boldsymbol{LQe}$
$\boldsymbol{e^-MJ}$ $\boldsymbol{eeMJ}$ $\boldsymbol{e\mu MJ}$ $\boldsymbol{\nu eMJ}$	$\boldsymbol{eMJ}$
$\boldsymbol{eeMJ}$ $\boldsymbol{e\mu MJ}$	$\boldsymbol{\nu eMJ}$
$\boldsymbol{\nu\mu MJ}$	$\boldsymbol{\nu MJ}$

Table 4: Prescription adopted to ensure no overlap between the considered channels.

The masses of the neutralinos, charginos and gluinos, as well as the couplings between any two SUSY particles and a standard fermion/boson, are determined by the usual MSSM parameters: the "mass" term μ which mixes the Higgs superfields, the SUSY soft-breaking mass parameters M_1, M_2 and M_3 for $U(1)$, $SU(2)$ and $SU(3)$ gauginos, and the ratio $\tan\beta$ of the vacuum expectation values of the two neutral scalar Higgs fields. These parameters are defined at the electroweak (EW) scale. We assume that the gaugino mass terms unify at a Grand Unification (GUT) scale to a common value $m_{1/2}$ leading to usual relations [4] between M_1, M_2 and M_3, and approximate the gluino mass by the value of M_3 at the EW scale. The masses and decay widths of all involved sparticles have been obtained using the SUSYGEN package.

For a fixed set of MSSM parameters and sfermion masses, the branching ratios for the different channels only depend on the Yukawa coupling. This also holds for the upper limit on the signal cross-section σ_{lim} derived from the combination of the analysed channels. At a given squark mass, Yukawa couplings for which σ_{lim} is smaller than the signal cross-section are excluded, where the signal cross-section is obtained by multiplying the leading-order production cross-section by K-factors [33] accounting for NLO QCD effects. These can enhance the signal rate by $\mathcal{O}(10\%)$.

Decay chains involving more than two SUSY fermions (χ or $\tilde{g}$) can contribute in principle to the gauge channels analysed. In these cases parameterising the signal efficiencies is not straightforward. Hence, only cascades involving two SUSY fermions are taken into account in the calculation of the visible branching ratios for gauge decay channels. This determination of the branching ratios is conservative. It has been checked that the visible branching is generally close to 100%. Decays of χ's into a Higgs boson are included in the calculation of the visible branching ratios when the Higgs decays into hadrons. The contribution of these decays is however very small. Hence the limits do not depend on the mass m_A of the pseudoscalar Higgs, set here to 300 GeV in the models where m_A is not related to the other parameters.

The case of a non-vanishing coupling λ'_{131} allowing for the resonant production of a stop squark (SUSY partner of the top quark) has to be treated separately. Firstly, the large top mass can not be neglected in the calculation of the branching ratios for the decays $\tilde{t} \rightarrow t\chi^0$ or $\tilde{t} \rightarrow t\tilde{g}$, which may eventually be kinematically forbidden. Secondly, the top quark decays via $t \rightarrow bW$. Most of the stop decays are in fact covered by our analysis, but the efficiencies for the considered channels, which are valid for decay patterns as shown in table 2, can not be used in that case. Conservatively, diagrams which lead to a top in the final state are thus not taken into account in the calculation of the visible branching ratios. For example, the $\not R_p$ decays $\chi_i^0 \to e^- t \bar{d}$ will not be included in the branching ratios for the $\boldsymbol{eMJ}$ and $\boldsymbol{e^-MJ}$ channels even when these are kinematically allowed. As a result, only the neutrino decays of the χ_i^0 ($\chi_i^0 \to \nu d \bar{d}$) will contribute in the derivation of limits on λ'_{131}.

6.2 Limits on λ'_{1j1} and λ'_{1j2} in the "phenomenological" MSSM

We consider here a version of the MSSM where the parameters μ, M_2 and $\tan\beta$ are only used to determine the masses and couplings of the χ's, while the sfermion masses are free parameters. We neglect any possible mixing between sfermions and assume that all squarks are degenerate in mass. This assumption only enters in the calculation of the branching ratios of the χ's and of the gluino, since we are mainly probing the $\tilde{u}_L^j$ squark. Sleptons are also assumed to be degenerate, and their mass $M_{\tilde{l}}$ is set either to the common squark mass, or to a fixed value (90 GeV) close to the lowest mass bound from sfermion searches at LEP. We first derive constraints on the couplings λ'_{1j1}, where a squark could be produced via an e^+d fusion, and consider in a second step squark production via e^+s fusion through a λ'_{1j2} coupling.

Example upper limits obtained at 95% confidence level (CL) on λ'_{1j1} ($j = 1, 2$) as a function of the $\tilde{u}_L^j$ mass are shown in Fig. 9a and Fig. 10a, under the assumption $M_{\tilde{l}} = 90$ GeV or $M_{\tilde{l}} = M_{\tilde{q}}$. The MSSM parameters are chosen such that the lightest neutralino is dominated by its photino component in Fig. 9 and by its zino component in Fig. 10. The gluino mass is large due to the large M_2 (and hence M_3) values and thus squark decays into $\tilde{g}$ are kinematically forbidden. In the four scenarios considered, Yukawa couplings larger than ~ 0.01 (~ 0.5) are ruled out for squark masses of 75 GeV (275 GeV).

The relative contributions of all channels are shown in Fig. 9b,c and Fig. 10b,c against the squark mass, at the current sensitivity limit on the Yukawa coupling. In each case the total branching ratio covered by the analysis is close to 100 $\%$. At the largest squark masses, where a large Yukawa coupling is necessary to allow squark production, the relative contribution of the $\boldsymbol{LQe}$ channel becomes important. In the case illustrated in Fig. 9 (Fig. 10) the dominant channels are those with an $e^\pm$ (ν) in the final state, resulting in particular from the main decay mode of the χ_1^0. The relative contributions of the channels strongly depend on the slepton mass. In the case illustrated in Fig. 9c, where a small slepton mass $M_{\tilde{l}} = 90$ GeV is used, the two-body decay of the ~ 95 GeV χ_1^+ or χ_2^0 into a lepton-slepton pair is kinematically allowed. As a result, the contributions of the channels $\boldsymbol{e\ell MJ}$ and $\boldsymbol{\nu\ell MJ}$ are considerably enhanced. In the case shown in Fig. 10, the channel $\boldsymbol{\nu MJ}$ remains dominant even in the light sleptons case because the χ_1^+ mass is here ~ 80 GeV. Only squark decays into the heavier χ_2^0 lead to the enhancement of the channel $\boldsymbol{\nu\ell MJ}$ shown in Fig. 10c.

Despite the fact that the relative contributions of the various channels are strongly model dependent, the upper limits on the Yukawa coupling do not depend significantly on the scenario considered because the sensitivity of our analysis is similar in all gauge channels, and because the covered branching ratio is always close to 100%.

In order to investigate more systematically how the sensitivity depends on the MSSM parameters, a scan of the parameters M_2 and μ is performed, for $\tan\beta = 2$. The effect of varying the parameter $\tan\beta$ will be studied in the next section. The mass of the sleptons is set to 90 GeV, the parameters M_2 and μ are varied in the range 70 GeV $< M_2 < 300$ GeV and -300 GeV $< \mu < 300$ GeV. Points which lead to a scalar LSP or to LSP masses below 30 GeV are not considered. This latter restriction, as well as the lower value for M_2, are motivated by the exclusion domains resulting from χ searches in $\not{R}_p$ SUSY at LEP. For each point in this (μ, M_2) plane the upper bound λ'_{lim} on the coupling λ'_{1j1} is obtained. The results are shown in Fig.11a for λ'_{1j1} $(j = 1, 2)$ and in Fig.11b for λ'_{131}. The two full curves in Fig.11 indicate the maximal and minimal values obtained for λ'_{lim} within the parameter space investigated.

The spread between these extrema for λ'_{lim} is small for squark masses above 150 GeV and decreases with increasing squark mass. Comparing Fig.11a and Fig.11b, the constraints on λ'_{131} and on λ'_{1j1} $(j = 1, 2)$ are seen to be quite similar. Only for small squark masses is the sensitivity on λ'_{131} reduced because of the small efficiency in the $\boldsymbol{\nu MJ}$ channel.

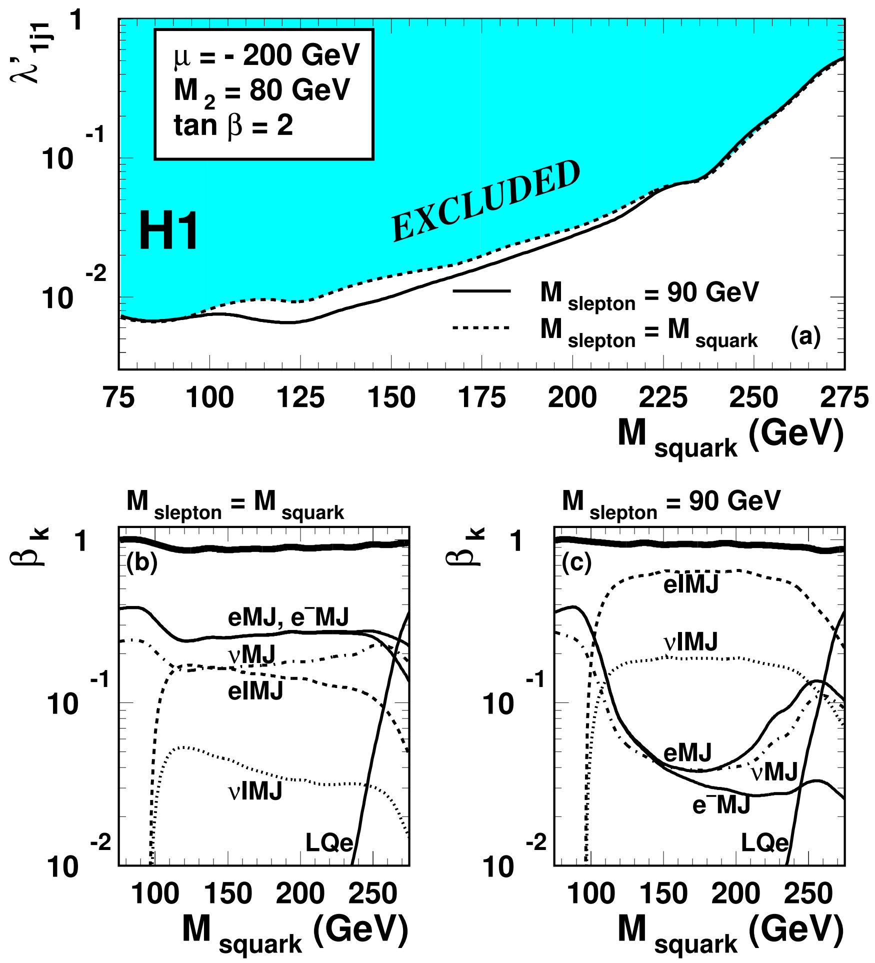

Figure 9: (a): Upper limits at 95% CL for the coupling λ'_{1j1} $(j = 1, 2)$ as a function of the squark mass, for a set of MSSM parameters leading to a χ_1^0 of ~ 40 GeV dominated by its photino component. Regions above the curves are excluded. The limits are given for two hypotheses on the slepton mass. (b): The branching ratios of all channels versus the squark mass, when sleptons and squarks are assumed to be degenerate; (c): as (b) but assuming a slepton mass of 90 GeV. The thick curves in (b) and (c) indicate the total branching covered by the analysis.

For a Yukawa coupling of electromagnetic strength ($\lambda'^2_{1j1}/4\pi = \alpha_{em}$, i.e. $\lambda'_{1j1} = 0.3$) squark masses below ~ 260 GeV are excluded at 95% CL . This extends beyond the mass domain excluded from relevant searches for scalar leptoquarks performed by the D0 [34] and CDF [35] experiments, which rule out $\tilde{u}^j_L$ squark masses below 205 GeV if the branching ratio of the squark into eq is greater than $\simeq 50\%$, and below ~ 110 GeV when this branching is $\sim 10\%$. Since in $\not{R}_p$ SUSY such a branching can be naturally small (as seen above) such leptoquark-like constraints are not very stringent. Direct squark searches at LEP exclude masses below ~ 90 GeV. Bounds from searches for $\not{R}_p$ SUSY carried out at the Tevatron do not apply in the unconstrained model considered here.

Our results are also compared in Fig. 11 to indirect limits [36]. The production of a $\tilde{u}$ squark via a λ'_{111} coupling is very severely constrained by the non-observation of neutrinoless double beta decay [37]. The best indirect limit on the coupling λ'_{121} (λ'_{131}), which could allow for the

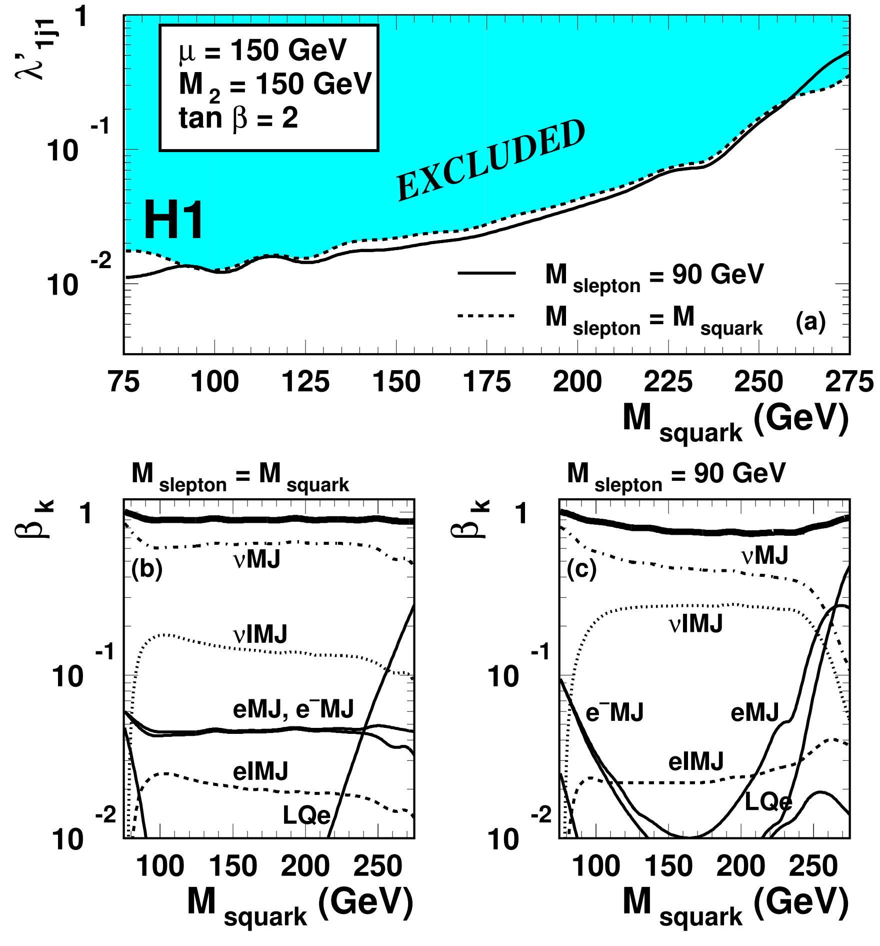

Figure 10: (a): Upper limits at 95% CL for the coupling λ'_{1j1} ($j = 1, 2$) as a function of the squark mass, for a set of MSSM parameters leading to a χ^0_1 of ~ 40 GeV dominated by its zino component. Regions above the curves are excluded. The limits are given for two hypotheses on the slepton mass. (b): The branching ratios of all channels versus the squark mass, when sleptons and squarks are assumed to be degenerate; (c): as (b) but assuming a slepton mass of 90 GeV. The thick curves in (b) and (c) indicate the total branching covered by the analysis.

production of squarks $\tilde{c}$ ($\tilde{t}$), comes from atomic parity violation (APV) measurements [36, 38]. For squark masses below ~ 240 GeV the H1 direct limits significantly improve this indirect constraint on λ'_{121} by a factor up to ~ 3. In the case of a non-vanishing λ'_{131} coupling, our results are more stringent than the APV constraints for stop masses between ~ 100 GeV and ~ 220 GeV.

The limits on the couplings λ'_{1j1} can be translated into upper bounds on the couplings λ'_{1j2}, which could allow for the production of a resonant $\tilde{u}^j_L$ via a fusion between the positron and a strange quark coming from the proton. To obtain the limit on λ'_{1j2} the ratio of the s and d quark densities and its uncertainty were taken from a LO QCD fit similar to [39], in which various neutrino DIS data providing constraints on $s(x)$ were considered. Resulting upper bounds at $M_{\tilde{q}} = 200$ GeV are shown in table 5. The limits were conservatively derived taking into account the 2σ uncertainties of the parton densities as given by the fit. Using the central prediction for $s(x)$ as given by the MRST parametrisation, limits on λ'_{1j2} do not change by more than 20%. Table 5 also shows existing indirect bounds [36] for comparison and recalls the bounds obtained on λ'_{1j1}. The sensitivity of our analysis to the coupling λ'_{132} is significantly better than that coming from the leptonic decay width of the Z boson. No attempt was made to derive limits on couplings λ'_{1j3} due to the large uncertainties on the b quark density at such high x and Q^2.

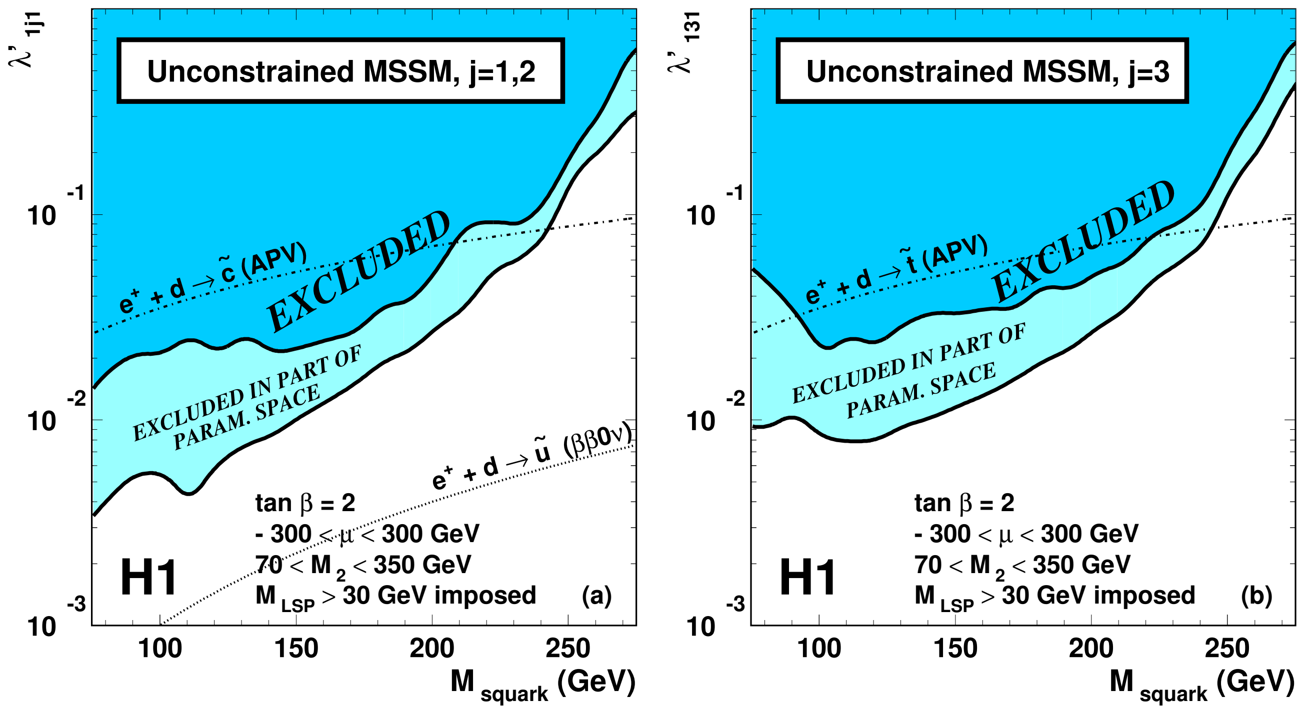

Figure 11: Upper limits at 95% CL on the coupling (a) λ'_{1j1} (j=1,2) and (b) λ'_{131} as a function of the squark mass for $\tan\beta = 2$, in the "phenomenological" MSSM. For each squark mass, a scan of the MSSM parameters M_2 and μ has been performed and the largest (lowest) value for the coupling limit is shown by the upper (lower) full curve. The dotted curve in (a) indicates the indirect bound on λ'_{111} from neutrinoless double beta decay assuming a gluino mass of 1 TeV. The dashed-dotted curves show the indirect bounds from atomic parity violation.

	λ'_{111}	λ'_{121}	λ'_{131}	λ'_{112}	λ'_{122}	λ'_{132}
λ'_{lim} (H1)	0.05	0.05	0.05	0.29	0.29	0.29
λ'_{lim} (indir.)	0.004	0.07	0.07	0.04	0.08	0.66
	$\beta\beta0\nu$	APV	APV	CC univ.	ν_e mass	$\Gamma(Z \to ll)$

Table 5: 95% CL upper bounds on the couplings λ'_{1j1} and λ'_{1j2} for a squark mass of 200 GeV. Also shown are the indirect bounds obtained from neutrinoless double beta decay, atomic parity violation, charged current universality, the upper bound on the neutrino mass, and the leptonic decay width of the Z boson.

6.3 Limits on λ'_{1j1} in the Constrained MSSM

In this section we consider a "constrained" (supergravity inspired) version of the MSSM where the number of free parameters is reduced by assuming, in addition to the GUT relation mentioned in section 6.1 between M_1, M_2 and M_3, a universal mass parameter m_0 for all sfermions at the GUT scale. The evolution of the sfermions masses towards low scales is given by the Renormalisation Group Equations (RGE) and depends on the gauge quantum numbers of the sfermions. As a result, the sfermions masses at the electroweak scale are related to each other and to the parameters determining the gaugino sector. The model is thus completely determined by e.g. m_0, M_2, μ and $\tan\beta$ (m_A is set to 300 GeV and we assume no mixing between the sfermions at the electroweak scale).

For a given value of the $\tilde{u}^j_L$ squark mass, the requirement of sfermion unification at large scale imposes an upper bound on the parameter M_2, which is obtained using approximate solutions for the RGE[5]. The upper bound on M_2 increases with the squark mass and is smaller for the stop than for other squarks. As before sets of parameters leading to a scalar LSP or to a LSP mass below 30 GeV are not considered. This lower bound on the LSP mass forbids too small values of M_2 and hence imposes a lower bound on the $\tilde{u}^j_L$ mass, which is more stringent in case of the stop. A scan of μ, $\tan\beta$ and M_2 is performed within -300 GeV $< \mu < 300$ GeV, $2 \leq \tan\beta \leq 40$ and within the M_2 range allowed by $\tan\beta$ and the $\tilde{u}^j_L$ mass.

The curves in Fig.12 indicate the maximal and minimal values for λ'_{lim} as a function of the $\tilde{u}^j_L$ mass. The spread of the domain spanned by the limits λ'_{lim} is quite small, i.e. the sensitivity of our analysis on λ' does not depend strongly on the free parameters of the model, in particular on $\tan\beta$. The most stringent limits are usually obtained for intermediate $\tan\beta$ and are in general better than those derived previously in the "unconstrained" MSSM because in this range the sneutrinos can be very light, leading to an enhancement of the quasi background-free channels $\boldsymbol{e\ell MJ}$ and $\boldsymbol{\nu\ell MJ}$ via e.g. $\chi^+_1 \to l^+\tilde{\nu}$.

For a Yukawa coupling of electromagnetic strength, squark masses up to values of $260-270$ GeV can be ruled out at 95% CL in the framework of the constrained MSSM. Moreover, for a coupling strength 100 times smaller than α_{em}, the most conservative bound on the mass of the $\tilde{u}^j_L$ obtained from the present analysis still reaches 182 GeV.

Searches for $R\!\!\!/_p$ SUSY performed at LEP [8] also set limits on the model considered here. At LEP the mass domain explored by direct searches for squarks with $R\!\!\!/_p$ couplings is limited by the beam energy. However searches for neutralinos and charginos lead to a lower bound on M_2 which, using the RGE's, can be translated into a lower bound of ~ 240 GeV on the squark mass, thus reducing the allowed mass domain probed in Fig.12 where only the less stringent

[5]The possible effect of the Yukawa couplings λ'_{1jk} on the RGE has not been taken into account here.

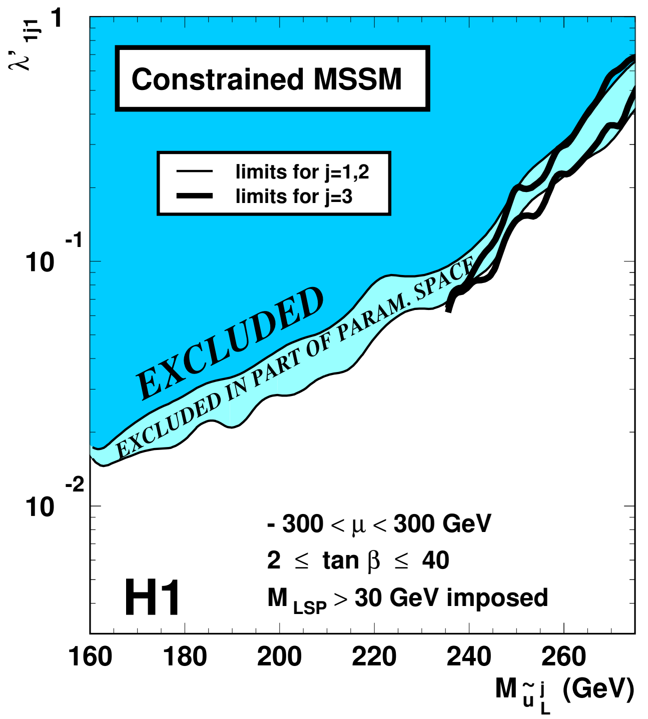

Figure 12: Upper limits at 95% CL for the coupling λ'_{1j1} as a function of the mass of the $\tilde{u}^j_L$, in the constrained MSSM. For each squark mass, a scan of the MSSM parameters μ, M_2 and $\tan\beta$ has been performed and the largest (smallest) value for the coupling limit is shown by the upper (lower) curve. The resulting band is contained within the thin curves for λ'_{1j1} ($j = 1, 2$) and within the thick ones for λ'_{131}. The requirement on the LSP mass imposes the $\tilde{u}^j_L$ to be heavier than ~ 160 GeV (~ 235 GeV) for $j = 1, 2$ ($j = 3$).

condition $M_{LSP} > 30$ GeV was imposed. The combined searches for χ's and sleptons at LEP moreover increase the lower M_2 bound for low values of the m_0 parameter. The resulting lower bound on the mass of first and second generation squarks is close to the current HERA centre of mass energy.

6.4 Constraints in the Minimal Supergravity Model

The model considered above can be further constrained by imposing a common SUSY soft-breaking mass term for all scalar fields, and by assuming that the breaking of the electroweak symmetry is driven by radiative corrections. These additional assumptions lead to the so-called *minimal* supergravity (mSUGRA) model [40]. By requiring Radiative Electroweak Symmetry Breaking (REWSB), the modulus of μ is related to the other model parameters. The program SUSPECT 1.2 [41] is used to obtain the REWSB solution for $|\mu|$ when the other parameters are fixed.

Assuming a fixed value for the $\not{R}_p$ coupling λ'_{1j1}, our searches can be expressed in terms of constraints on the mSUGRA parameters, for example on $(m_0, m_{1/2})$ when $\tan\beta$, the common trilinear coupling at the GUT scale A_0, and the sign of μ are fixed. The parameter A_0 enters only marginally in the interpretation of the results and A_0 is set to zero. Values of the parameters leading to a LSP lighter than 30 GeV have not been excluded here. However a vanishing efficiency has been assumed for squarks undergoing a gauge decay ending by a χ or $\tilde{g}$ lighter than 30 GeV, since the parametrisation of the efficiencies (see section 4) is not valid in this domain.

For $\tan\beta = 2$ and $\mu < 0$, results obtained for a Yukawa coupling $\lambda'_{1j1} = 0.3$ ($j = 1, 2$) are shown in the $(m_0, m_{1/2})$ plane in Fig. 13a. The parameter space where $M_{\tilde{u}^j_L} < 260$ GeV

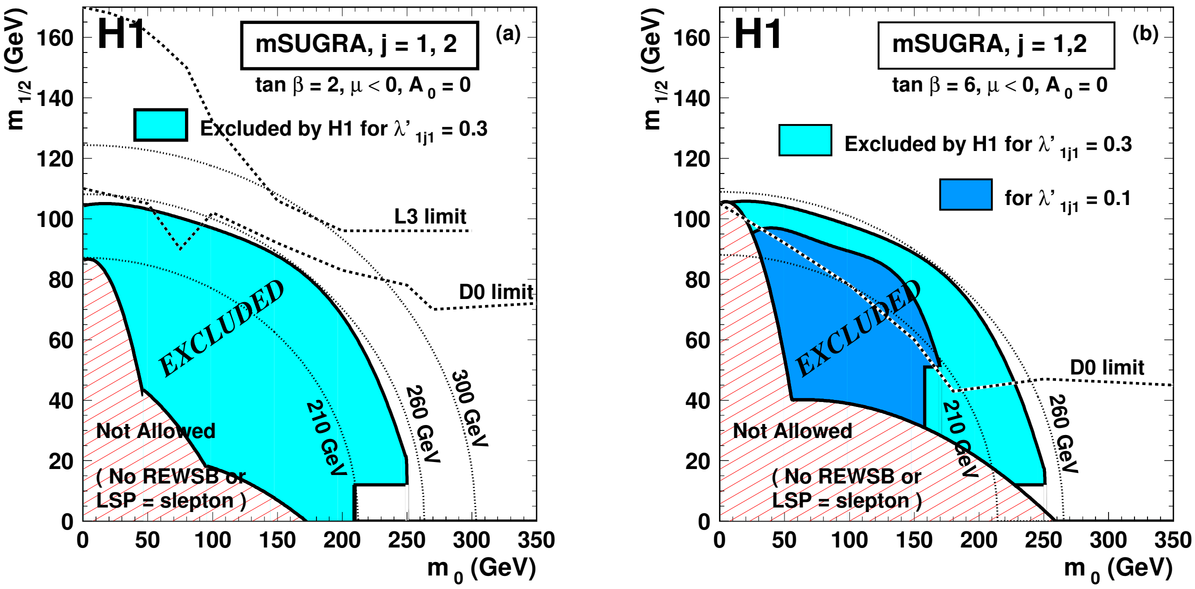

Figure 13: Domain of the plane $(m_0, m_{1/2})$ excluded by this analysis for $\mu < 0$, $A_0 = 0$ and (a) $\tan\beta = 2$ or (b) $\tan\beta = 6$, for a $\not{R}_p$ coupling $\lambda'_{1j1} = 0.3$ ($j = 1, 2$) (light shaded areas). In (b) the exclusion domain obtained for $\lambda'_{1j1} = 0.1$ ($j = 1, 2$) is also shown as the dark grey area. The hatched domains correspond to values of the parameters where no REWSB is possible or where the LSP is a sfermion. The regions below the dashed curves are excluded by the D0 experiment; in (a) also the L3 bound is shown as the dashed-dotted curve; these limits do not depend on the value of the $\not{R}_p$ coupling. Two isolines for the mass of the $\tilde{u}^j_L$ are also shown as dotted curves.

is nearly fully excluded. At low $m_{1/2}$ values where the lightest χ's and the $\tilde{g}$ are lighter than 30 GeV, the sensitivity on the $\tilde{u}^j_L$ mass however decreases since the efficiency is conservatively set to zero for all channels but $\boldsymbol{LQe}$, and reaches ~ 210 GeV. Fig. 13a also shows the domain excluded by the D0 experiment [42] from searches for SUSY where R_p is violated by a λ'_{1jk} coupling, relying on di-electron events. H1 and Tevatron results are quite similar at low m_0. However, the mSUGRA parameter space is still more constrained by the combined searches for χ's and sleptons carried out at LEP as shown in Fig. 13a. LEP and Tevatron bounds do not depend on the value of the Yukawa coupling.

Results for $\tan\beta = 6$ and $\lambda'_{1j1} = 0.3$ or 0.1 ($j = 1, 2$) are shown in Fig. 13b. The excluded domains extend considerably beyond the region ruled out by the D0 experiment. This is due to the fact that, for large values of $\tan\beta$, the lightest neutralino is dominated by its zino component, so that its decay into $e^{\pm}$ is suppressed. As a result the sensitivity of the di-electron D0 analysis is decreased, while the dominant squark decay mode is still observable in the H1 analysis via the $\boldsymbol{\nu MJ}$ and $\boldsymbol{\nu\ell MJ}$ channels. LEP limits in [8] have not been given for this value of $\tan\beta$ but the corresponding bounds on $m_{1/2}$ are expected to be similar to those shown in Fig. 13a within ~ 10 GeV.

We now consider a non-vanishing coupling λ'_{131} which could lead to the production of a stop. The weak interaction eigenstates $\tilde{t}_L$ and $\tilde{t}_R$ mix in this case through an angle θ_t to form two mass eigenstates, labelled $\tilde{t}_1$ and $\tilde{t}_2$ ($\tilde{t}_1$ being the lightest by convention):

$$\begin{pmatrix} \tilde{t}_1 \\ \tilde{t}_2 \end{pmatrix} = \begin{pmatrix} \cos\theta_t & \sin\theta_t \\ -\sin\theta_t & \cos\theta_t \end{pmatrix} \begin{pmatrix} \tilde{t}_L \\ \tilde{t}_R \end{pmatrix}$$

The production cross-section of the $\tilde{t}_1$ ($\tilde{t}_2$) scales as $\lambda'^2_{131}\cos^2\theta_t$ ($\lambda'^2_{131}\sin^2\theta_t$) since only $\tilde{t}_L$ enters in the $L_1Q_3\bar{D}_1$ operator. Hence, the lightest stop $\tilde{t}_1$ does not necessarily have the largest production cross-section. Thus both $\tilde{t}_1$ and $\tilde{t}_2$ are searched for in the analysis.

For channels $\boldsymbol{e^-MJ}$, $\boldsymbol{e\ell MJ}$ and $\boldsymbol{\nu\ell MJ}$ where the signal is integrated over the whole mass range the fraction of the visible signal in a given channel, k, is $\sum_{i=1,2}\beta_{k,i}\varepsilon_{k,i}\sigma_i/\sigma_{tot}$, where $\beta_{k,i}$ is the branching ratio for $\tilde{t}_i$ to decay into this channel k, $\varepsilon_{k,i}$ the corresponding selection efficiency, σ_i the production cross-section of $\tilde{t}_i$, and $\sigma_{tot} = \sigma_1 + \sigma_2$ the total signal cross-section.

For the channels $\boldsymbol{LQe}$, $\boldsymbol{eMJ}$ and $\boldsymbol{\nu MJ}$ where the signal is integrated over a "sliding mass bin" only the contribution of the state $\tilde{t}_i$ for which the sensitivity is maximal (i.e. which maximises $\sigma_i(\sum_k \beta_{k,i}\varepsilon_{k,i})$) is taken into account in the above summation. The numbers of observed and expected events are then integrated in the mass bin corresponding to $\tilde{t}_i$ only.

The results are shown in Fig. 14 for $\lambda'_{131} = 0.3$, $A_0 = 0$, $\mu < 0$ and $\tan\beta = 2$ or $\tan\beta = 6$. The domain below the line $m_{1/2} \lesssim 10$ GeV is not considered since it corresponds to cases where the only allowed LSP decay into $\nu b\bar{d}$ is kinematically forbidden. For $\tan\beta = 2$, the excluded domain is slightly larger than that ruled out previously for $\lambda'_{1j1} = 0.3$ ($j = 1, 2$), due to the mixing in the stop sector which leads to $\tilde{t}_1$ masses smaller than the masses of the other $\tilde{u}^j_L$ squarks. In particular, larger values of m_0 can be probed. This remains the case for $\tan\beta = 6$ as long as $m_{1/2}$ is large enough to ensure that the mass of the lightest neutralino is above 30 GeV. When the χ^0_1 becomes too light, the efficiencies for the channels involving a $\chi^+_1 \to \chi^0_1$ decay are set to zero, and the sensitivity to the signal is only provided by the $\boldsymbol{LQe}$ channel or by the decays $\tilde{t} \to b\chi^+_1$ followed by a $\not{R}_p$ decay of the chargino. As a result, only lighter stops can be probed, for which the visible cross-section is large enough. Note that for both values of $\tan\beta$, masses of $\tilde{t}_1$ up to 245 GeV can be excluded for $\lambda'_{131} = 0.3$. This is slightly smaller than the maximal sensitivity of ~ 260 GeV reached, for the same coupling value, on the $\tilde{u}^j_L$ ($j = 1, 2$) mass (Fig. 13), or on the $\tilde{t}_L$ mass in the constrained MSSM when the stop mixing is neglected (Fig. 12). This is due to the $\cos^2\theta_t$ reduction of the $\tilde{t}_1$ cross-section.

For intermediate values of m_0, the L3 sensitivity is slightly better than the limit obtained from this analysis for $\tan\beta = 2$. In the same part of the parameter space, the H1 limit is comparable with or slightly extends beyond the expected LEP sensitivity for $\tan\beta = 6$.

7 Conclusions

We have searched for squarks in e^+p collisions at HERA in R-parity violating SUSY models. No evidence for the resonant production of such particles was found in the various channels considered which cover almost all decay modes. Mass dependent limits on R-parity violating

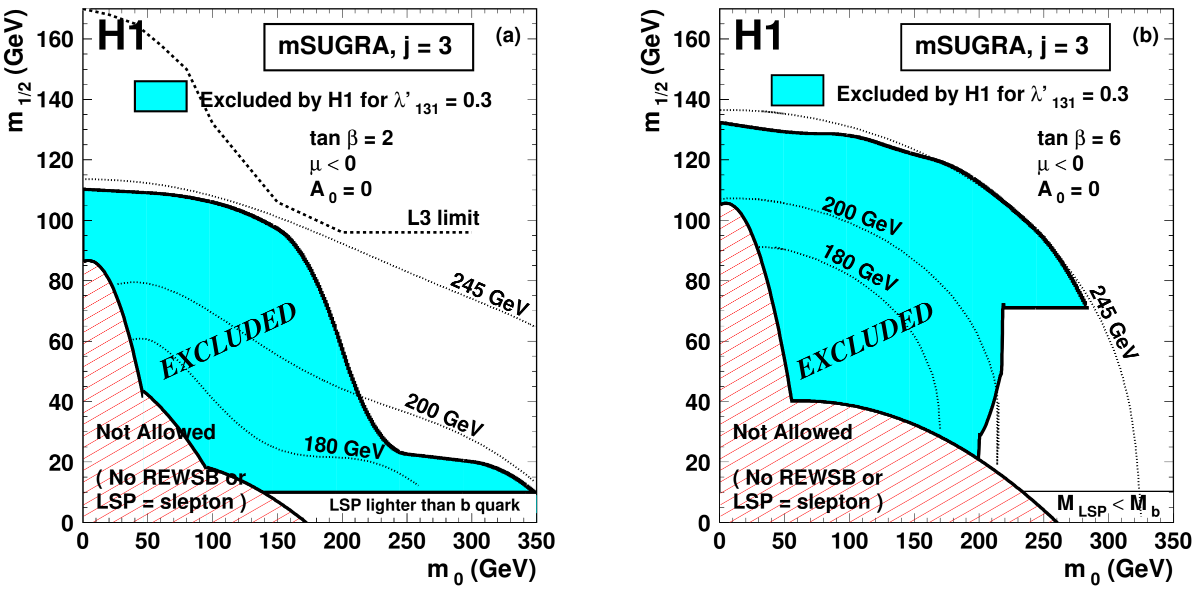

Figure 14: Domain of the plane $(m_0, m_{1/2})$ excluded for a $\not{R}_p$ coupling $\lambda'_{131} = 0.3$, for $\mu < 0$, $A_0 = 0$ and (a) $\tan\beta = 2$ or (b) $\tan\beta = 6$. The hatched domains on the left correspond to values of the parameters where no REWSB is possible or where the LSP is a sfermion. For too small $m_{1/2}$ (the domain below the line $m_{1/2} \sim 10$ GeV), the LSP becomes lighter than the b quark and thus is stable for a non-vanishing λ'_{131} coupling. The region below the dashed curve in (a) is excluded by the L3 experiment; this limit does not depend on the value of the $\not{R}_p$ coupling. Three isolines for the mass of the $\tilde{t}_1$ are shown as dotted curves.

couplings were derived. The limits were set within the unconstrained MSSM, the constrained MSSM and the minimal Supergravity model. The model dependence of the results was studied in detail by performing a scan of the MSSM parameters and was found to be small.

In the large part of the MSSM parameter space covered by the scan, the existence of squarks coupling to an e^+d pair with masses up to 260 GeV is excluded at 95% confidence level for a strength of the Yukawa coupling equal to α_{em}. For a 100 times smaller coupling strength squark masses below 182 GeV are ruled out. This improves the indirect bounds set by low-energy experiments and, in SUSY models where the sfermion and the gaugino sectors are not related, extends beyond the reach of other collider experiments. In models where the sfermion masses depend on the parameters which determine the supersymmetric gauge sector, the limits extend beyond the constraints obtained at the Tevatron collider for intermediate values of $\tan\beta$ and for a Yukawa coupling of electromagnetic strength, and are comparable with LEP bounds in part of the parameter space.

Acknowledgements

We wish to thank the HERA machine group as well as the H1 engineers and technicians who constructed and maintained the detector for their outstanding efforts. We thank the funding agencies for their financial support. We wish to thank the DESY directorate for the support and hospitality extended to the non-DESY members of the collaboration. We thank the members of the French “Groupement de Recherche en Supersymétrie” for useful discussions, for their help in adapting the SUSYGEN generator to ep collisions and for providing the SUSPECT program.

References

[1] C. Adloff *et al.* [H1 Collaboration], Eur. Phys. J. **C11** (1999) 447 [hep-ex/9907002].

[2] S. Aid *et al.* [H1 Collaboration], Z. Phys. **C71** (1996) 211 [hep-ex/9604006].

[3] T. Ahmed *et al.* [H1 Collaboration], Z. Phys. **C64** (1994) 545.

[4] H. P. Nilles, Phys. Rept. **110** (1984) 1;
H. E. Haber and G. L. Kane, Phys. Rept. **117** (1985) 75.

[5] J. Butterworth and H. Dreiner, Nucl. Phys. **B397** (1993) 3 [hep-ph/9211204] and references therein.

[6] W. Buchmüller, R. Rückl and D. Wyler, Phys. Lett. **B191** (1987) 442 and *Erratum* Phys. Lett. **B448** (1999) 320.

[7] DELPHI Collaboration, DELPHI 2000-072, submitted to the XXX Int. Conf. on High Energy Physics, Osaka, Japan (27 July - 2 August 2000).

[8] M. Acciarri *et al.* [L3 Collaboration], CERN-EP-130 (2000), submitted to Eur. Phys. J. C. [hep-ex/0011087].

[9] I. Abt *et al.* [H1 Collaboration], Nucl. Instrum. Meth. **A386** (1997) 310.

[10] B. Andrieu *et al.* [H1 Calorimeter Group Collaboration], Nucl. Instrum. Meth. **A336** (1993) 460.

[11] B. Andrieu *et al.* [H1 Calorimeter Group Collaboration], Nucl. Instrum. Meth. **A350** (1994) 57;
B. Andrieu *et al.* [H1 Calorimeter Group Collaboration], Nucl. Instrum. Meth. **A336** (1993) 499.

[12] R. D. Appuhn *et al.* [H1 SPACAL Group Collaboration], Nucl. Instrum. Meth. **A386** (1997) 397.

[13] J. Ban *et al.* [H1 BEMC Group Collaboration], Nucl. Instrum. Meth. **A372** (1996) 399.

[14] DJANGO 6.2; G.A. Schuler and H. Spiesberger, Proc. of the Workshop Physics at HERA, W. Buchmüller and G. Ingelman (Editors), (October 1991, DESY-Hamburg) Vol. 3 p. 1419.

[15] G. Gustafson and U. Pettersson, Nucl. Phys. **B306** (1988) 746;
idem, *addendum* Lund University preprint LU-TP-87-19, (October 1987) 4pp.;
B. Andersson, G. Gustafson, L. Lönnblad and U. Pettersson, Z. Phys. **C43** (1989) 625.

[16] L. Lönnblad, Comput. Phys. Commun. **71** (1992) 15.

[17] T. Sjöstrand, Lund Univ. preprint LU-TP-95-20 (August 1995) 321pp;
idem, CERN TH-7112 (1993) [hep-ph/9508391].

[18] A. D. Martin, R. G. Roberts, W. J. Stirling and R. S. Thorne, Eur. Phys. J. **C4** (1998) 463 [hep-ph/9803445].

[19] PYTHIA 5.7; T. Sjöstrand, CERN-TH-6488 (1992);
T. Sjöstrand, Comput. Phys. Commun. **82** (1994) 74.

[20] M. Glück, E. Reya and A. Vogt, Phys. Rev. D **45** (1992) 3986;
M. Glück, E. Reya and A. Vogt, Phys. Rev. D **46** (1992) 1973.

[21] LEGO 0.02; K. Rosenbauer, PhD. thesis, RWTH Aachen (in German), PITHA 95/16 (July 1995).

[22] I. Abt *et al.* [H1 Collaboration], Nucl. Phys. **B396** (1993) 3;
S. Aid *et al.* [H1 Collaboration], Phys. Lett. **B369** (1996) 173 [hep-ex/9512001].

[23] S. Katsanevas and P. Morawitz, Comput. Phys. Commun. **112** (1998) 227 [hep-ph/9711417].

[24] SUSYGEN 3.0/0.6, "A Monte Carlo Event generator for MSSM sparticle production for e^+e^-, $\mu^+\mu^-$ and ep colliders", N. Ghodbane, S. Katsanevas, P. Morawitz and E. Perez, http://lyoinfo.in2p3.fr/susygen/susygen3.html;
E. Perez, Proceedings of the Workshop "Monte Carlo Generators for HERA Physics", DESY, 1998-1999, p 635, A.T. Doyle, G. Grindhammer, G. Ingelman and H. Jung (Editors).

[25] V. N. Gribov and L. N. Lipatov, Sov. J. Nucl. Phys. **15** (1972) 438;
G. Altarelli and G. Parisi, Nucl. Phys. **B126** (1977) 298;
Y. L. Dokshitzer, Sov. Phys. JETP**46** (1977) 641.

[26] C. Adloff *et al.* [H1 Collaboration], Eur. Phys. J. **C13** (2000) 609 [hep-ex/9908059].

[27] A. Blondel, F. Jacquet, Proceedings of the Study of an ep Facility for Europe, ed. U. Amaldi, DESY report 79-48 (1979) 391.

[28] C. Adloff *et al.* [H1 Collaboration], Z. Phys. **C74** (1997) 191 [hep-ex/9702012].

[29] J. Breitweg *et al.* [ZEUS Collaboration], Eur. Phys. J. **C16** (2000) 253 [hep-ex/0002038].

[30] J. Breitweg *et al.* [ZEUS Collaboration], DESY 00-133, to be published in Phys. Rev. D [hep-ex/0009059].

[31] H. L. Lai *et al.*, Phys. Rev. D **55** (1997) 1280 [hep-ph/9606399].

[32] A. Arbuzov, D. Bardin, J. Bluemlein, L. Kalinovskaya and T. Riemann, Comput. Phys. Commun. **94** (1996) 128 [hep-ph/9511434].

[33] T. Plehn, H. Spiesberger, M. Spira and P. M. Zerwas, Z. Phys. **C74** (1997) 611 [hep-ph/9703433].

[34] B. Abbott *et al.* [D0 Collaboration], Phys. Rev. Lett. **79** (1997) 4321 [hep-ex/9707033];
B. Abbott *et al.* [D0 Collaboration], Phys. Rev. Lett. **80** (1998) 2051 [hep-ex/9710032].

[35] F. Abe *et al.* [CDF Collaboration], Phys. Rev. Lett. **79** (1997) 4327 [hep-ex/9708017].

[36] H. Dreiner, published in "Perspectives on Supersymmetry" (1997), Ed. G.L. Kane, World Scientific, p 462 [hep-ph/9707435].

[37] R. N. Mohapatra, Phys. Rev. D **34** (1986) 3457;
J. D. Vergados, Phys. Lett. **B184** (1987) 55;
M. Hirsch, H. V. Klapdor-Kleingrothaus and S. G. Kovalenko, Phys. Lett. **B352** (1995) 1 [hep-ph/9502315];
M. Hirsch, H. V. Klapdor-Kleingrothaus and S. G. Kovalenko, Phys. Rev. Lett. **75** (1995) 17;
M. Hirsch, H. V. Klapdor-Kleingrothaus and S. G. Kovalenko, Phys. Rev. D **53** (1996) 1329 [hep-ph/9502385].

[38] P. Langacker, Phys. Lett. **B256** (1991) 277.

[39] V. Barone, C. Pascaud and F. Zomer, Eur. Phys. J. **C12** (2000) 243 [hep-ph/9907512].

[40] M. Drees and M. M. Nojiri, Nucl. Phys. **B369** (1992) 54;
H. Baer and X. Tata, Phys. Rev. D **47** (1993) 2739;
G. L. Kane, C. Kolda, L. Roszkowski and J. D. Wells, Phys. Rev. D **49** (1994) 6173 [hep-ph/9312272].

[41] SUSPECT 1.2, code written by A. Djouadi, J.L. Kneur and G. Moultaka.

[42] B. Abbott *et al.* [D0 Collaboration], Phys. Rev. Lett. **83** (1999) 4476 [hep-ex/9907019].